UNLIMITED

TR 89048

TR 89048

ROYAL AEROSPACE ESTABLISHMENT

Technical Report 89048

November 1989

RE - ANALYSIS OF DATA ON THE SPACE RADIATION ENVIRONMENT ABOVE SOUTH - EAST ASIA

by

P. R. Truscott

Procurement Executive, Ministry of Defence
Farnborough, Hampshire

"original contains color plates: All DTIC reproductions will be in black and white"

UNLIMITED

0072340

CONDITIONS OF RELEASE

BR-113987

****

DRIC U

****

DRIC Y

Reports quoted are not necessarily available to members of the public or to commercial organisations.

UNLIMITED

ROYAL AEROSPACE ESTABLISHMENT

Technical Report 89048

Received for printing 8 September 1989

RE-ANALYSIS OF DATA ON THE SPACE RADIATION ENVIRONMENT ABOVE SOUTH-EAST ASIA

by

P. R. Truscott

SUMMARY

A new analysis has been performed on the HRM-III gamma ray detector data collected from Shuttle missions STS-41B, 41C, 41D, 41G and 51A. The new analysis shows no evidence for the existence of enhanced levels of radiation in low-Earth orbit over South-East Asia (*ie* in the area bounded by longitudes 100°E to 190°E and latitudes 10°S to 15°N) as previously suggested. Variations in the detector count rates with geographical location are shown to be consistent with the variation of the cosmic ray flux with geomagnetic latitude, and also show expected increases due to the South Atlantic Anomaly (SAA) and outer belt electrons. However, at times poor quantitative agreement is found between the expected positions of the SAA or outer electron belt, and the Shuttle's geographical location on the occasions when high count rates were observed. It is believed that this lack of correlation is a result of the sensitivity of the trapped particle environment to geographical position and magnetospheric activity.

Departmental Reference: Space 677

UNLIMITED

LIST OF CONTENTS

1 INTRODUCTION

Radiation Monitoring Equipment (RME) experiments have been carried out on Shuttle missions STS-41B, 41C, 41D, 41G and 51A. One of the monitoring devices flown was a hand-held, gamma ray counter (HRM-III) which for the purposes of these experiments was programmed to detect ionising radiation over a total period of 52.5 minutes, 'binning' the number of counts detected at 30 second intervals. The HRM-III was operated in the cabin area four times during each mission, with the exception of STS-41D when the detector was operated six times during flight.

Analysis of the results performed by Madonna *et al*[1] and Cash *et al*[2], of the US Air Force Technical Applications Center, showed that higher levels of radiation appeared to have been experienced when Shuttle was located geographically near to the equator and between longitudes 100°E and 190°E. These high levels of radiation were stated to be due to a *South-East Asian radiation anomaly* (SEAA).

In this report the HRM-III data has been re-analysed, and the results examined and compared with expected cosmic ray and trapped particle variations related to the Shuttle's geographical location.

RAE Space Department's interest in the Shuttle cabin radiation environment stems from its plans to fly on Shuttle a comprehensive, mid-deck, radiation dosimetry experiment called CREAM (Cosmic Radiation Effects and Activation Monitor)[3]. The aims of the CREAM experiment are to provide data to improve:

(a) knowledge of the radiation environment outside a spacecraft;

(b) predictive software for modelling radiation transport in spacecraft materials;

(c) software used to predict single event upset phenomena in microelectronics and the background levels in sensors for future spacecraft.

The study of the RME data was therefore undertaken to primarily determine the cause of the apparent radiation anomaly, but also to:

(a) provide valuable information about the Shuttle cabin radiation environment;

(b) obtain experience in dealing with data from Shuttle missions (as some of the analysis techniques will also be applicable to the CREAM experiment) and define some of the important experimental parameters for CREAM which may have been under-estimated or overlooked.

2 RADIATION DETECTION IN SPACE

2.1 The HRM-III gamma ray counter

The HRM-III is a hand-held, gamma ray counter which uses a mercuric iodide crystal as the detection medium. The detection threshold of the crystal is 100 keV. The counter detects each gamma event through the photocurrent produced in the crystal as a result of ionisation and pair production by the gamma rays. Therefore, the detector will also be activated by other ionising particles, namely charged particles, this provided they deposit sufficient energy.

The counter circuitry is all solid state and is microprocessor controlled. One hundred and five memories are used to store the number of counts detected at specified time intervals. This interval may be varied from 1/3 to 33 seconds, but for the purposes of the RME experiments was set at 30 seconds for all missions, giving a total collection time of 52.5 minutes or approximately 60% of a typical Shuttle orbit.

At the end of the collection period the data in each of the memories was displayed on the monitor's LCD display and recorded by the astronaut 'with pen and paper'.

2.2 Sources of radiation above 100 keV in the spacecraft environment

The sources of primary radiation which may be detected in low-Earth orbit (LEO) by the HRM-III are:

(a) Primary gamma rays and X-rays

These are produced within our own and other galaxies by nuclear and electromagnetic processes in stars (and the Sun) and the interstellar medium. However, this primary gamma radiation constitutes only a small fraction of the total radiation experienced, and in comparison with other sources may be neglected.

(b) Galactic cosmic rays

The ability of these highly energetic nuclei to reach LEO depends on the particle's momentum-to-charge ratio, or rigidity, and the combined shielding effects of the geomagnetic field and the Earth.

At the equator the nuclei have to cross a large number of magnetic field lines and may be deflected back into space before the detector is reached, whereas nearer the poles there is less magnetic shielding. Therefore, for a given altitude above the Earth, more cosmic rays are detected when over the geomagnetic poles than at the equator, and to a first approximation this

variation is given by a restricted version of the Störmer equation, which describes the vertical cut-off rigidity for particles moving in a pure dipole field as a function of distance from the dipole centre (r) and the magnetic latitude (λ):

$$P_v(r,\lambda) \propto \frac{\cos^4\lambda}{r^2} \quad . \tag{1}$$

This vertical cut-off rigidity is the minimum rigidity a particle must have to reach the point at (r,λ), approaching the point along the direction of the radius vector , $-\mathbf{r}$. Since one may consider the Earth's field to be nearly dipolar, this equation represents a reasonable first approximation, but better approximations have been made using trajectory integration techniques, which take into account the effects of the higher order terms in the geomagnetic field (quadrupole, octapole, etc) and the Earth's shadow (Shea and Smart[4]).

(c) The Van Allen radiation belts

These consist predominantly of electrons and protons trapped by the geomagnetic field in the magnetosphere. The particles trace eccentric helices, travelling approximately along the field lines, until the magnetic field becomes sufficiently strong to reflect or 'mirror' them (see Fig 1). As a result, the particles oscillate back and forth between the Northern and Southern hemispheres.

Again the levels of radiation detected depend on the geomagnetic and hence the geographical location. Figs 2 and 3 show contours of constant omnidirectional trapped proton and electron flux respectively, observed in a plane containing the geomagnetic North-South axis[5]. Both particle flux intensities increase with distance from the Earth when at LEO type altitudes. Also, it can be seen that, whereas the proton flux is maximum at one location near the equatorial line (at approximately 3 Earth radii or 3 R_e), the electrons are formed into two zones: an inner belt with an equatorial flux maximum at approximately 1.5 R_e and an outer belt with a maximum at 5 R_e. Two regions of intense trapped electron radiation for LEO are the 'horns' of the outer belt. In these areas electrons from the outer zone mirroring at low altitudes intersect a high inclination orbit at high latitudes in the Northern and Southern hemispheres.

Because the Earth's dipole is displaced from the geographical centre by about 480 km towards the central Pacific Ocean, the trapped particles mirror at a lower altitude on the opposite side of the Earth, *ie* when roughly over the South Atlantic. For a low-inclination LEO the highest fluxes of trapped protons and electrons will therefore be experienced when in this area. This is the so-called South **Atlantic** Anomaly (or SAA).

All the above primary radiations are modified by their passage through the spacecraft, and in undergoing nuclear and electromagnetic interactions with the spacecraft materials (and the detector itself) can produce secondary particles, which themselves undergo further interactions. Therefore the HRM-III will also detect:

(a) Secondary protons and heavier nuclei, neutrons and pions ejected from the nuclei of the spacecraft material through intra-nuclear cascades of the cosmic rays and trapped protons.

(b) Gamma rays emitted from in-elastic nuclear scattering of secondary neutrons.

(c) Prompt gamma rays and delayed or induced radioactivity (gammas, betas, etc) associated with the gradual decay of spalled nuclei.

(d) Muons from the decay of charged pions, and gamma rays produced as neutral pions undergo self-annihilation. The muons themselves may decay to produce electrons and positrons, and all these particles (muons, electrons, positrons and gammas) can undergo electromagnetic interactions with spacecraft materials producing an *electromagnetic* cascade of photons, electrons and positrons. The high energy of cosmic rays causes pions to be frequently created and also gives rise to high multiplicity of secondary particles (electrons, photons, etc), therefore for cosmic rays these interactions represent an important source of secondary radiation.

(e) Photons, electrons and positrons produced through electromagnetic interactions of trapped electrons with materials.

To summarise, the effects of primary gamma radiation on the total number of particles counted will be small in comparison with those due to galactic cosmic rays and trapped radiation and their secondaries. The amount of primary and secondary radiations detected will depend on the levels of shielding afforded by Shuttle, but the intensities of the trapped, cosmic and secondary radiations are still expected to be highly correlated with geomagnetic location.

2.3 Why a South-East Asian radiation anomaly is not expected

Because of the nature of the geomagnetic field, one would not at first expect high particle fluxes to be detected in a LEO over South-East Asia (between latitudes 10°S to 15°N and longitudes 100°E to 190°E) as found by Madonna *et al*[1] and Cash *et al*[2]. In simple terms to argument is as follows:

A detector positioned above South-East Asia will be at its closest point to the Earth's dipole centre (for a given altitude). As a result, the degree of shielding provided by the geomagnetic field is highest in this area (see equation (1)) and therefore the cosmic ray flux should be at a minimum. The close proximity of the dipole centre also means that trapped particles will be mirroring at higher altitudes than for other longitudes. If the longitude of the detector is changed it should experience an increase in the trapped particle flux. Moving the detector North or South at typical Shuttle altitudes, could in priciple lead to a decrease in flux, until the outer electron belt (the 'horns') is reached. However, the proton and electron fluxes are very tenuous in the South-East Asian region (<1 particle $cm^{-2}s^{-1}$ for protons with energies >10 MeV, and electrons >1 MeV), and measurements of the variation of particle flux in this area are usually more affected by cosmic rays.

It is therefore surprising that Madonna *et al* and Cash *et al* found evidence to the opposite, although this is not the first report of enhanced levels of radiation detected above South-East Asia. It was noted by Elliot[6] that the Anton 302 Geiger-Müller counter flown on UK Ariel I detected similar high levels of radiation between latitudes 0° and 20°N and longitudes 100°E and 160°E. However, in that case it was concluded that the enhanced count rates were the result of induced radioactivity in the detector and surrounding spacecraft materials after passing through the SAA. Three features of this 'South-East Asian Anomaly' supported this view:

(a) Count rates from the G-M counter were taken only near equator crossings, and due to Ariel's particular orbit, ground-tracks that crossed the equator in South-East Asia also had to pass through the SAA (see Fig 4).

(b) The count rates experienced above South-East Asia were found to be at a maximum when the satellite was at perigee (see Fig 5), which required the satellite to have previously been at apogee when in the SAA, and consequently exposed to the highest trapped proton fluxes for the orbit.

(c) A spare detector was irradiated with proton fluences comparable to those which might be experienced in the SAA. The level of induced radioactivity measured after 50 minutes (roughly the time taken for the satellite to travel

from apogee to perigee) was in good agreement with the count rates observed on the spaceborne detector at the second equator crossing.

In the case of the RME experiments, induced radioactivity is unlikely to be the cause of the enhanced count rates observed simply because the average count rates increase on approaching the South-East Asian Anomaly instead of decreasing from the SAA to the region of this second amomaly.

3 RESULTS AND DESCRIPTION OF ANALYSIS TECHNIQUES USED

3.1 Orbital analysis

Figs 6 to 12 show the HRM-III detector data plotted as a function of Shuttle's longitude together with the spacecraft's ground-track for the period the detector was on. In order to obtain these ground-tracks, the six Keplerian elements describing the spacecraft's location were determined at 30 second intervals from the start of operation of the HRM-III by extrapolating, to the desired time, orbital elements published by NASA Goddard Space Flight Center. The extrapolation allowed for perturbations in the orbit due to the J_2 term in the Earth's gravitational potential, and more details are given in Appendix A.1.

In most cases there is good agreement between the ground-tracks shown in Figs 6 to 12 and the predictions for Shuttle's geographical location made by Madonna *et al*[1] and Cash *et al*[2]. However, large discrepancies are present in some cases, including those where the South-East Asian Anomaly was said to have been observed, or some other unexpected variation of count rate with geomagnetic latitude was experienced. Table 1 lists these cases together with approximate geographical locations where the HRM-III was switched on, and where the peaks in the count rates were observed.

From this new orbital analysis it can be seen that there is a more consistent correlation between the detector data and Shuttle location - the peaks in the count rates occur when Shuttle is at or near to the Northern or Southern-most point in its orbit, and therefore when cosmic ray effects should be most apparent (see section 2.2). However, there is one exception, and that is the fifth operation of the detector during mission STS-41D.

The start times for the detection periods are given in Table 2. It can be seen that the mission elapsed time (MET) for the start of the second operation of the HRM-III on STS-41B was not known by the author of this report, and since the original analysis did not show signs of a SEAA, no results are presented here for this particular run. For the fifth operation of the HRM-III during STS-41D, the MET day does not at first sight appear to have been recorded by the astronaut.

In order to produce the ground-track shown in Fig 9, therefore, it was assumed that the data was collected on the fourth day into the mission (*ie* MET = 04/04:03:36), which is in agreement with the start times for the fourth and sixth experiments for that mission (see Table 2). If, however, it is assumed that the *recorded time* (04:03:36) did in fact include the date and was supposed to mean 04/03:36:xx, one obtains a ground-track which passes through the heart of the SAA at the time when very high count rates were recorded (see Fig 10).

Figs 13 and 14 summarise the cases where inconsistencies between the present and the original orbital analyses are apparent, and once again, there appears to be better qualitative agreement (when the corrected orbits are used) between the detector count rates and the expected geographical variation of the radiation environment, as described in section 2.2.

3.2 Analysis of cosmic ray effects

From Figs 6 to 14 it can be seen that there is a strong correlation between the detector count rate and geographical/geomagnetic latitude. However, both the cosmic ray intensity and trapped particle fluxes change with geomagnetic latitude. Therefore, to help assess the relative contributions of these two radiation sources the HRM-III data has been plotted as a function of vertical cut-off rigidity (see Figs 15 to 24).

The vertical cut-off rigidities were determined by extrapolating from a grid of trajectory-derived cut-offs (Shea and Smart[4]) calculated at 15.0° longitude and 5.0° latitude intervals at an altitude 20 km above the mean Earth surface. To perform the extrapolation it was assumed that the cut-off varied according to the Störmer equation over small changes in radial distance from the magnetic dipole centre (δr) and geomagnetic latitude ($\delta\lambda$), *ie*:

$$\delta P_v = - P_v \left\{ 2 \frac{\delta r}{r} + 4 \tan \lambda \delta\lambda \right\} \qquad (2)$$

as suggested by Smart and Shea[7]. Further details about the methods used in this extrapolation are given in Appendix A.2.

Figs 15 to 24 show that, although there is some variation in the count rate (*ie* greater than the expected Poisson statistical error) for a given cut-off rigidity, there is reasonable correlation between the count rate and the rigidity.

For the fourth operation of the HRM-III on STS-41C there is some uncertainty in the last digit of the initial MET (see Table 2). The start time of 5/16:08:00 was chosen as it was within the limits of uncertainty and fitted the general variation of count rate with vertical cut-off rigidity found from the other results.

Figs 18 to 21 show some additional features. For operations #2 and #5 of Shuttle mission STS-41D (Figs 18 and 19) peaks in the detector count rate occur at a rigidity of ≈1 GV, suggesting a change in the nature of the main radiation source. These peaks correspond well to when the spacecraft is in the SAA area (see Figs 8 and 10) and hence where trapped particle effects may begin to dominate. Similarly, operations #1 and #3 of the HRM-III during STS-41G (57° inclination) again show deviations which may correspond to Shuttle passing through the 'horns' of the outer electron belt; note for example the peaks at 2 GV, 3 GV and 8 GV in Fig 20 (operation #1) and 0.5 GV and 1 GV in Fig 21 (operation #3). The results from operations #2 and #4 during STS-41G show a generally more consistent variation of count rate with cut-off rigidity. In Fig 22 the data for these two operations have been re-plotted, together with data obtained from a lower inclination orbit mission (STS-41B, operation #1).

A feature which appears to be characteristic in almost all these graphs is that, for a given operation of the detector, two count rates can be associated with a given vertical cut-off rigidity. This is perhaps most clearly seen in Fig 15 in the results for mission STS-41B. In fact such a change in count rate should be expected since the cut-off rigidity for cosmic rays varies as a function of the direction in which they approach a detector, as well as the detector's geographical location, and a larger number of cosmic rays are found to approach a detector from the direction of magnetic West[8]. So, although at two different locations above the Earth the vertical cut-off rigidity may have been the same, the orientation of Shuttle with respect to magnetic West would most likely have been different, depending on the attitude control mode being executed by the spacecraft. Therefore, different levels of shielding would have been afforded to the detector from the anisotropic radiation, changing the count rates experienced. However, it is still uncertain why there appears to be two fairly well defined count rates for one vertical cut-off rigidity (as shown in Fig 15) and not a spread of count rates with set upper and lower limits, as would be expected.

These facts suggest that, for most of the Shuttle orbit time, the main contribution to the radiation detected by the HRM-III comes from primary cosmic rays and the secondary particles produced by their interactions with the spacecraft

materials. At certain times other sources begin to dominate the detector count rate, and a further analysis was performed to determine how well these features corresponded to the enhanced trapped radiation levels of the SAA and the 'horns' of the outer electron belt.

3.3 Analysis of trapped particle effects

In Figs 25 to 36 the HRM-III data have been plotted against time from the start of the experiment, together with the predicted instantaneous trapped proton and electron fluxes. These estimates for the trapped particle fluxes were calculated using the ESA UNIRAD suite of programmes[9-11]. Conversion from the geographical to geomagnetic coordinates (or 'B-L' space) was performed using the IGRF 1980 model for the geomagnetic field extrapolated to the launch dates for the Shuttle missions. The AP8MIN[12] and AE8MIN[13] models for the trapped particle environment were then used to determine the proton and electron flux levels respectively at these locations in the orbit.

In Fig 25 (STS-41D, HRM-III operation #2) the peak in the detector data at 7 minutes is in good agreement with a rise in the proton flux as Shuttle passes through the South Atlantic Anomaly. The second maximum at 17 minutes does not appear to be clearly resolved from the rise in the cosmic ray flux as the spacecraft nears the Southern-most point in its orbit. Similarly, enhancements in the electron flux (Fig 26) do not appear to be sufficient to be detected above the effects of the other radiation sources. The sharp peak in the predicted proton flux at 4.5 minutes is not present in the HRM-III data, and appears to reflect the sensitivity of the flux levels derived from the models to geographical location.

In Figs 27 and 28 (STS-41D, operation #5) the increase in the count rate between 24 and 48 minutes (originally believed to be due to the South-East Asian Anomaly) agrees qualitatively with the enhanced proton and electron flux levels predicted from crossing the SAA. There is similar agreement for other SAA and outer electron belt traversals:

Figs 29 and 30 (STS-41G, operation #1)

Figs 33 and 34 (STS-41G, operation #3)

However, for mission STS-41G there are clearly several cases where a significant increase in the count rate is observed, when Shuttle is near its Northern-most point and may be in the outer electron belt zone, but no corresponding increase in electron flux is predicted. Also there exist cases when

trapped particle enhancement is predicted, but no corresponding increase in count rate is detected, for example:

Figs 31 and 32 (STS-41G, operation #2) at 20 and 48 minutes

Fig 35 (STS-41G, operation #4) at 3 minutes

To summarise, the results of this particular analysis show that certain increases in the detector count rates correspond well to times when enhanced trapped proton and electron flux levels are expected. There are, however, discrepancies which are likely to be a result of the sensitivity of the trapped radiation levels to geographical location (see section 4.3).

3.4 Geomagnetic and magnetospheric activity

Table 3 lists the geomagnetic activity indicies for the periods of the Shuttle missions. Forbush decreases (FD) in the neutron data measured at ground stations at Thule (290.80°E, 77.50°N) and Huancayo (284.70°E, 12.00°S) have been listed. The percentage decrease in the neutron count rates were evaluated using the formula:

$$\Delta R = \frac{\left\{\begin{matrix}\text{previous day}\\ \text{count rate}\end{matrix}\right\} - \left\{\begin{matrix}\text{present day}\\ \text{count rate}\end{matrix}\right\}}{\left\{\begin{matrix}\text{average count}\\ \text{rate for month}\end{matrix}\right\}} \times 100(\%) \quad . \qquad (3)$$

No significant variations in the cosmic-ray/secondary particle intensities appear to have been detected by the HRM-III during the recovery phase of the Forbush event of 3/2/84 (see Fig 15). However, the events of 7/4/84 (STS-41C, operation #1) and 15/11/84 (STS-51A, operation #4) may be the cause of the lower count rates shown in Figs 16 and 24 respectively. In Fig 20 (STS-41G, operation #1) the 'baseline' count rate observed, when Shuttle is not subjected to intense trapped radiation, is noticeably lower than the 'baseline' count rates for the other operations of the detector. Again this may be as a result of the FD which occurred on that day.

For low-inclination LEO the trapped particle environment would not have been significantly affected by the geomagnetic/magnetospheric activity. For higher inclination orbits during these periods of activity, as in the case of mission STS-41G, large fluctuations in the outer belt electrons can take place. This factor would have contributed to the lack of correlation between the predicted electron flux levels and the observed count rates, as in operations #2 and #4 of the HRM-III.

4 UNCERTAINTIES AND SOURCES OF ERROR

4.1 Orbital analysis

There are several possible sources of error involved in determining the location of Shuttle corresponding to each of the 105 count 'bins' during each operation of the HRM-III:

(a) The launch times for the missions. These were obtained from readily available space mission data and are accurate to ±1 minute. Accuracy greater than this was not believed necessary in the light of the next source of error.

(b) The times recorded for the start of each run. Again these are typically no worse than ±1 minute, with the exception of the fourth operation of the HRM-III on STS-41C where there is some uncertainty in the last digit of the recorded MET giving a maximum error of 10 minutes (for this experiment the initial MET was assumed to be 5/16:08:00).

(c) The extrapolation of the NASA GSFC published orbital elements to the times during which the detector was operated. To assess the accuracy of the J_2 orbital dynamics model used for this extrapolation, a comparison was made between this orbital data and predictions published by NASA GSFC in the 30 Day Prediction Bulletins. Table 4 lists the longitude and time differences between the two orbital predictions for when Shuttle is near its Northern/Southern-most point in the orbit or at the equator.

Since the extrapolation was usually performed over less than 8 hours, agreement between the two predictions was found to be good. Typically discrepancies in longitude are less than 2°, which could at most give rise to a maximum error in latitude (when near the equator) of 1.1° for a 28.5° orbit, and 3.1° for a 57° orbit. Differences in the predicted times for equator crossings are usually less than 30 seconds, and no greater than 3.2 minutes.

4.2 Analysis of cosmic ray effects

The errors involved in determining the vertical cut-off rigidities for the time the detector was active come from:

(a) Uncertainty in the geographical location of Shuttle described in section 4.1.

(b) The first order extrapolation of the grid of trajectory-derived data to the spacecraft location, and the assumption that the Earth's magnetic field can be approximated to an eccentric dipole in order to apply the Störmer equation.

The suitability of correlating the detector data with only the *vertical* cut-off rigidity may also be questioned since the cut-off rigidity varies significantly with the direction with which the particles approach the detector. Variations in detector count rate have been observed (section 3.2) which appear to be the result of changes in Shuttle's orientation with respect to the anisotropic cosmic ray flux. Clearly it is desirable that any future analysis considers the variation in the cosmic ray flux with repect to the spacecraft body coordinates, together with the different shielding effects afforded by Shuttle for the particles approaching from the different directions.

4.3 Analysis of trapped particle effects

In this part of the analysis, sources of error come from:

(a) Uncertainty in the geographical location of Shuttle, and hence its position in geomagnetic or 'B-L' space. This is most significant for the near-polar regions reached by the orbit of STS-41G. Uncertainty in the latitude of approximately ±1° can lead to an error in the magnetic shell number (L) of ±1. This may have contributed to the low degree of correlation between the HRM-III data and the predicted electron fluxes.

(b) Both the proton and electron models used (AP8MIN and AE8MIN) were derived for the trapped particle environment at solar minimum, and these were chosen for the analysis as the Shuttle missions took place nearer the period of solar minimum than solar maximum.

(c) The proton and electron models are averaged and static models (in B-L space). As mentioned in section 3.4 significant fluctuations in the outer belt electrons can be expected as a result of the geomagnetic activity during STS-41G.

Finally, when geomagnetic field models are extrapolated into the future, they all predict a decrease in the Earth's field strength and hence a lowering of the altitude at which the trapped particles mirror. This effect by itself would lead to an increase in the flux levels experienced at a given altitude, but in LEO it is counteracted by a rise in the absorption rate of the particles in the atmosphere. This attenuation by the atmosphere is not accounted for by the particle or field models and therefore using a field model which has been extrapolated to the epoch of a future mission (in the 1990s say) produces excessively high flux level predictions.

To overcome this McCormack[14] has suggested using a geomagnetic field model which has been extrapolated back to the epoch of the trapped particle model being

used. However, this technique was not adopted for the analysis presented in this report, since:

(a) In this analysis the AP8MIN and AE8MIN models were being extrapolated only to 1984.

(b) Whilst McCormack's suggestion is highly applicable to situations where the *mission-averaged dose* rate is desired, for this analysis the variation of flux with geographical location (and hence B-L space) was required. Also, only a qualitative comparison between the flux levels predicted by the models and the detector count rates has been made.

5 CONCLUSIONS

The data obtained from the HRM-III gamma ray detector flown on several Shuttle missions have been re-analysed and a new orbital analysis, based on data from NASA Goddard Space Flight Center, has been performed. The analysis does not support the existence of a South-East Asian radiation anomaly (SEAA) as previously reported, and shows that at the times of the observations the spacecraft was in different geographical locations to those which had been previously calculated. With the new orbit data, all the observed 'SEAA' enhancements in the detector count rate can be adequately explained in terms of the expected variation in cosmic ray flux with geomagnetic latitude, and the effects of the South Atlantic Anomaly (SAA).

Cosmic radiation dominates the observed count rate when outside the SAA and the 'horns' of the outer electron belt. The shielding of Shuttle against these cosmic rays also appears to play an important role, as the count rate has been found to vary for a given vertical cut-off rigidity.

The periods of enhanced count rates coincide qualitatively with when Shuttle is in the SAA or the 'horns' of the outer electron belt. A comparison between the times of the observed enhancements and the expected instantaneous trapped proton and electron fluxes (based on the AP8MIN and AE8MIN models) shows good quantitative temporal agreement in some cases, but poor correlation in others, especially when near the outer electron zone.

This study has resulted in a greater understanding of the radiation environment to which low altitude spacecraft are exposed, and hence will allow more accurate modelling of the radiation-dependent degradation of spacecraft components and systems and will indicate how longer life missions may be achieved.

6 RECOMMENDATIONS

There should be a further analysis to determine the contribution to the HRM-III count rate due to trapped radiation. This analysis would involve taking into account the variation of the cut-off rigidity of the cosmic ray flux with the spacecraft body coordinates, and the shielding effects of Shuttle. Then by subtracting the expected contribution due to cosmic rays from the total count rate, the effect of the trapped particle radiation can be determined.

In the forthcoming RAE experiments using the CREAM package of dosimeters, there should be particular attention to the following parameters:

(a) Accurate and frequent orbital data, especially if the Shuttle mission chosen is for a high inclination orbit.

(b) Attitude or orientation of Shuttle with respect to magnetic West.

(c) Detector location in Shuttle, and the degree of shielding afforded by the spacecraft at that location.

Acknowledgments

The author would like to acknowledge the assistance of C.C. Kelleher and A.N. Winterbottom with useful discussions on the subjects of orbital dynamics and Shuttle operations, and J.P. Sleath for providing information concerning the trapped radiation environment. The author would also like to thank A. Balogh (of Imperial College of Science, Technology and Medicine, London) for suggesting the area of research and for his many helpful comments.

Appendix

ANALYSIS TECHNIQUES

A.1 Orbital analysis methods

The elliptical orbit of a spacecraft, and the position of the spacecraft within the orbit, can be represented by the six Keplerian elements, namely:

Two coordinates to define the ellipse:

a - semi-major axis of the ellipse;

e - eccentricity.

Three coordinates to define the orientation of the ellipse:

i - inclination of the plane of the ellipse to the Earth's equatorial plane;

Ω - right ascension of the ascending node;

ω - argument of perigee - the angle between the ascending node and perigee.

One coordinate to define the position of the spacecraft within the ellipse:

M - mean anomaly - which is defined as:

$$M = 2\pi \times \frac{\text{(time since last at perigee)}}{\text{(orbital period)}} \quad . \tag{A-1}$$

To a first approximation (*ie* if only the monopole term in the Earth's gravitational field is considered and all other forces are neglected) all the above coordinates remain constant with time, except for M , which varies at a constant rate with time. However, the non-spherical shape of the Earth gives rise to perturbations in the shape and orientation of the ellipse which (to a good approximation) causes a constant precession of the right ascension of the orbit and the argument of perigee. The changes in Ω and ω per orbit are given by[15]:

$$\Delta\Omega = - \frac{3\pi J_2 \cos i}{\left(\frac{a}{R}\right)^2 (1 - e^2)^2} \tag{A-2}$$

$$\Delta\omega = \frac{3\pi J_2 (4 - 5 \sin^2 i)}{2\left(\frac{a}{R}\right)^2 (1 - e^2)^2} \qquad \text{(A-3)}$$

where J_2 is a measure of the ellipsoidal shape of the Earth, and R is the mean equatorial radius of the Earth with values:

$$J_2 = 1.08265 \times 10^{-3}$$

$$R = 6378.160 \text{ km} .$$

This correction of the right ascension and argument of perigee is the so-called J_2 approximation.

A.2 Method used to determine the vertical cut-off rigidities

Vertical cut-off rigidities have been calculated by Shea and Smart[4] using trajectory integration techniques. These rigidities were calculated at a grid of points 20 km above the mean Earth surface, at intervals of 5° in latitude and 15° in longitude for the epoch of 1975.0. In order to extrapolate the vertical cut-offs to other geographical locations, it was assumed that the rigidity varied according to the Störmer equation (Smart and Shea[7]) and that, to a first approximation, this change in rigidity is given by:

$$\delta P_v \simeq - P_v \left\{ 2 \frac{\delta r}{r} + 4 \tan \lambda \delta\lambda \right\} \qquad \text{(A-4)}$$

where δr is the change in distance from the dipole centre, and $\delta\lambda$ is the change in magnetic latitude. An eccentric dipole model approximation for the geomagnetic field was used (Chapman and Bartels[16]) based on the first eight terms of the IGRF 1980 field model, extrapolated to the launch date of each mission.

To improve the estimate of the vertical cut-off rigidity, the rigidities at the four points on the grid which were nearest in longitude and latitude were each extrapolated to the new point, and a weighted mean of all four values taken. The weighting scheme was chosen to be in relation to the distance between the grid point and the new point, with the weight W_i applied to the i^{th} grid point calculated from the expression:

$$W_i = \begin{cases} \dfrac{1.0}{\left\{ \dfrac{|\text{long} - \text{long}_i|}{15.0} + \dfrac{|\text{lat} - \text{lat}_i|}{5.0} \right\}} & : \text{provided } < 20.0 \\ 20.0 & : \text{otherwise} \end{cases} \qquad \text{(A-5)}$$

where (long, lat) = longitude and latitude of new point

$(\text{long}_i, \text{lat}_i)$ = longitude and latitude of i^{th} grid point.

An upper limit of 20.0 for the weight was chosen arbitrarily to avoid over-emphasis on a particular grid point.

If P_i is the vertical cut-off rigidity of the i^{th} grid point and $\delta P_i(\delta r, \delta\lambda)$ is the change in rigidity when going to the new grid point, then the weighted mean is given by:

$$\bar{P} = \frac{\sum_i \left\{ P_i + \delta P_i(\delta r, \delta\lambda) \right\} W_i}{\sum_i W_i} \quad . \qquad \text{(A-6)}$$

Table 1

HRM-III OPERATIONS WHERE A SOUTH-EAST ASIAN ANOMALY (SEAA) OR OTHER DISCREPANCIES IN THE DATA WERE NOTED IN PREVIOUS ANALYSIS

Mission	HRM-III Operation	Old analysis Start Pt		'Anomaly' Pt		New analysis Start Pt		'Anomaly' Pt	
STS-41B	#1(SEAA)	65°E	17°N	187°E	5°S	338.5°E	19.6°N	90.9°E	28.2°S
STS-41D	#2	228°E	28°N	258°E	22°N	305.6°E	4.7°S	329.4°E	17.1°S
STS-41D	#4(SEAA)	350°E	12°N	172°E	2°S	67.9°E	28.6°S	253.0°E	27.8°N
STS-41D	#5(SEAA)	50°E	25°S	145°E	13°N	307.2°E	16.3°S	56 7°E	15.7°S
STS-41D*	#5(SEAA)					209.5°E	27.5°N	306.8°E	16.2°S
STS-41D	#6(SEAA)	342°E	23°S	107°E	6°N	66.9°E	5.4°S	189.5°E	25.1°N
STS-51A	#1	39°E	5°S	201°E	10°N	117.7°E	28.3°S	277.6°E	28.6°N

* Initial MET of 04/03:36:00 assumed.

Table 2

DATES AND TIMES OF SHUTTLE LAUNCHES AND OPERATION OF HRM-III DETECTOR

Mission	Launch time (GMT)	Run	Start of operation MET	GMT	
STS-41B	3 Feb 84 13:00 ± 00:01	#1	0/22:55:00	4 Feb	11:55:00
(STS-10)		#2	(NDA)	(NDA)	
		#3	5/00:35:30	8 Feb	13:35:30
		#4	6/18:47:00	10 Feb	07:47:00
STS-41C	6 Apr 84 13:59 ± 00:01	#1	0/20:20:xx	7 Apr	10:19:00
		#2	2/18:10:xx	9 Apr	08:09:00
		#3	3/19:08:xx	10 Apr	09:07:00
		#4	5/16:0x:xx	12 Apr	06:07:00
STS-41D	30 Aug 84 12:42 ± 00:01	#1	1/02:03:45	31 Aug	14:45:45
		#2	2/03:43:00	1 Sep	16:25:00
		#3	2/19:38:xx	2 Sep	08:20:00
		#4	3/23:46:xx	3 Sep	12:28:00
		#5	4/04:03:36	3 Sep	16:45:36
		#6	5/04:40:00	4 Sep	17:22:00
STS-41G	5 Oct 84 11:03 ± 00:01	#1	1/06:44:26	6 Oct	17:47:26
		#2	2/03:30:00	7 Oct	14:33:00
		#3	5/05:50:00	10 Oct	16:53:00
		#4	7/02:50:00	12 Oct	13:53:00
STS-51A	8 Nov 84 12:15 ± 00:01	#1	0/23:27:00	9 Nov	11:42:00
		#2	2/21:39:30	11 Nov	09:54:30
		#3	4/19:35:00	13 Nov	07:50:00
		#4	6/18:03:00	15 Nov	06:18:00

Dates and times of start of operation of HRM-III recorded by astronaut (MET) have been added to the launch time to produce the start of operation time in GMT.

NDA indicates no data was available.

Table 3

GEOMAGNETIC ACTIVITY INDICES DURING DETECTOR OPERATION

Mission	HRM-III Operation	Kp	Day Sum of Kp	Forbush decreases Date	Thule	Huancayo
STS-41B	#1	6-	41+	3/2/84	2.0%	0.5%
	#3	2	16-			
	#4	2	25			
STS-41C	#1	6	28+	7/4/84	0.8%	1.1%
	#2	3	31-			
	#3	2-	16-			
	#4	2	22			
STS-41D	#1	3	20+			
	#2	2	19-			
	#3	3-	20			
	#4	2-	20-			
	#5	2-	20-			
	#6	8-	26+	4/9/84	0.7%	
STS-41G	#1	3	26+	6/10/84	2.5%	1.0%
	#2	6	37			
	#3	4	32			
	#4	3	33+			
STS-51A	#1	2	21			
	#2	4-	26+			
	#3	2-	17-			
	#4	3+	39	15/11/84	0.8%	0.4%

Table 4

COMPARISON BETWEEN J_2 MODEL AND NASA GSFC PREDICTIONS OF SHUTTLE GEOGRAPHICAL POSITION

Mission	HRM-III Operation	Event	Error in time (s)	Error in longitude (degrees)
STS-41B	#1	NS	10.0	-1.1
	#1	S	28.0	-0.1
	#3	NS	2.0	-1.0
	#3	S	-4.0	-1.2
	#4	S	-5.4	-1.8
	#4	SN	3.0	-1.3
STS-41C	#1	S	19.2	-0.2
	#1	SN	-3.1	-1.0
	#2	SN	-0.3	-1.0
	#2	N	5.4	-0.6
	#3	S	13.8	-0.1
	#3	SN	-0.3	-1.0
	#3	N	4.8	-0.7
	#4	NS	-5.0	-1.0
	#4	S	-6.0	-1.9
STS-41D	#1	NS	-13.3	-0.9
	#1	S	-7.8	-0.4
	#1	SN	-17.1	-0.9
	#2	S	-63.6	-1.0
	#2	SN	-61.3	-0.7
	#3	N	-82.2	-0.8
	#3	NS	-79.5	-0.7
	#4	S	46.2	-1.6
	#4	SN	49.8	-1.2
	#4	N	34.2	-2.0
	#5	NS	14.3	-1.1
	#5	S	2.4	-1.7
	#6	SN	-4.7	-1.0
	#6	N	1.2	-1.2
	#6	NS	4.8	-1.0
STS-41G	#1	N	189.8	-0.3
	#1	NS	147.1	-1.6
	#2	N	-3.0	-0.9
	#2	NS	-3.9	-1.0
	#3	N	9.0	-0.5
	#3	NS	4.0	-1.0
	#3	S	13.8	-0.6
	#4	S	-31.2	-2.5
	#4	SN	24.2	-1.1
STS-51A	#1	SN	1.3	-1.0
	#1	N	-4.8	-1.3
	#2	NS	3.7	-1.0
	#2	S	-8.4	-1.7
	#3	S	-15.0	-0.6
	#3	SN	-21.3	-0.9
	#4	N	-8.4	-1.6
	#4	NS	0.1	-1.0

Error (or difference) = (J_2 model prediction) - (NASA GSFC prediction).

SN or NS signify Shuttle at equator, crossing South-North or North-South respectively, N or S signify Shuttle at Northern-most or Southern-most point in orbit.

REFERENCES

No.	Author	Title, etc
1	R.G. Madonna V.L. Brown S.E. Cash	Results from radiation monitoring equipment experiment on STS-11. US Air Force Technical Applications Center Report AFTAC-TR-85-2 (1985)
2	S.E. Cash R.G. Madonna M.R. McClellan M.E. Fields	Results from radiation monitoring equipment experiments on STS-41C, 41D, 41G, and 51A. US Air Force Technical Applications Center Report AFTAC-TR-85-4 (1985)
3	C.S. Dyer A.J. Sims R.J. Hutchings D. Mapper J.H. Stephen J. Farren	The Cosmic Ray Effects and Activation Monitor. Royal Aircraft Establishment Technical Memo TM 364 (1988)
4	M.A. Shea D.F. Smart	A five by fifteen degree world grid of calculated cosmic ray vertical cutoff rigidities for 1965 and 1975. 14th International Cosmic Ray Conference, Vol 14, 1298-1303 (1975)
5	A. Holmes-Siedle R. Freeman	Radiation effects engineering handbook. Final report for ESA contract 2871/76/NL/HP Fulmer Research Institute report R730/8 (1978)
6	H. Elliot	Some cosmic ray and radiation belt observations based on the data from the Anton 302 G-M counter in Ariel I. From 'Radiation Trapped in the Earth's Magnetic Field' Edited by Billy M. McCormac, Reidel (1966)
7	D.F. Smart M.A. Shea	analysis of trajectory derived penumbral widths. 14th International Cosmic Ray Conference, Vol 14, 1309-1314 (1975)
8	A.E. Sandström	Cosmic ray physics. p 115-116, North-Holland Publishing Co, Holland (1965)
9	J.Cl. Debruyn L.H. Jensen	The UNIFLUX system. ESTEC Working PAPER 1308 (1983)

REFERENCES (concluded)

No.	Author	Title, etc
10	A.J. Sims	Software for the prediction of spacecraft exposure to the Van Allen radiation belts. Royal Aircraft Establishment Working Paper SP (87) WP 7 (1987)
11	E.G. Stassinopoulos J.J. Herbert E.L. Butler J.L. Barth	NASA NSSDC/WDC-A-R&S, 79-01 (1979)
12	D.M. Sawyer J.I. Vette	AP8 trapped proton environment for solar maximum and solar minimum. NSSDC/WDC-A-R&S, 76-06, NASA-GSFC, TMX-72605 (1976)
13	M.J. Teague J.I. Vette	AE5 - A model of the trapped electron population for solar minimum. NASA-GSFC (1974)
14	P.D. McCormack	Radiation dose and shielding for the space station. IAF/IAA-86-380 (1986)
15	R.W. Wolverton	Flight performance handbook for orbital operators. John Wiley & Sons inc (1963)
16	S. Chapman J. Bartels	Geomagnetism, Vol 2. Oxford Clarendon Press (1940)

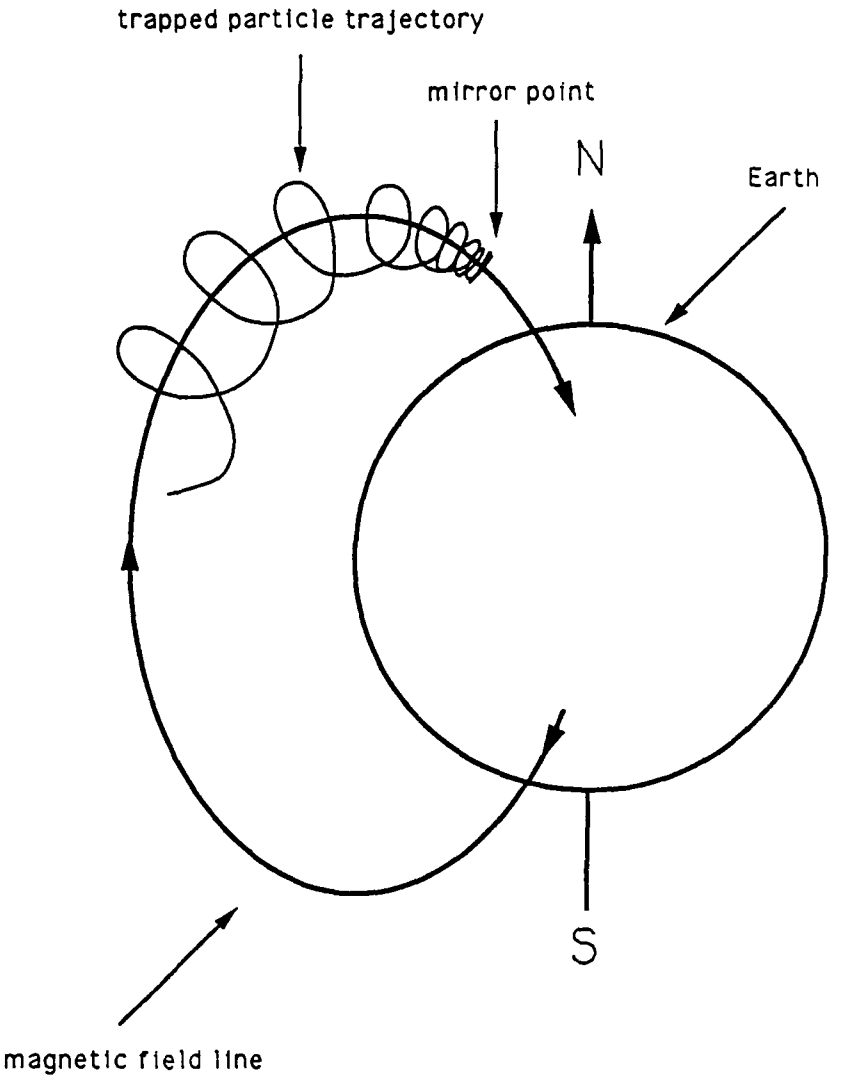

TR 89048

Fig 1 Example of trajectory of particle trapped in the geomagnetic field

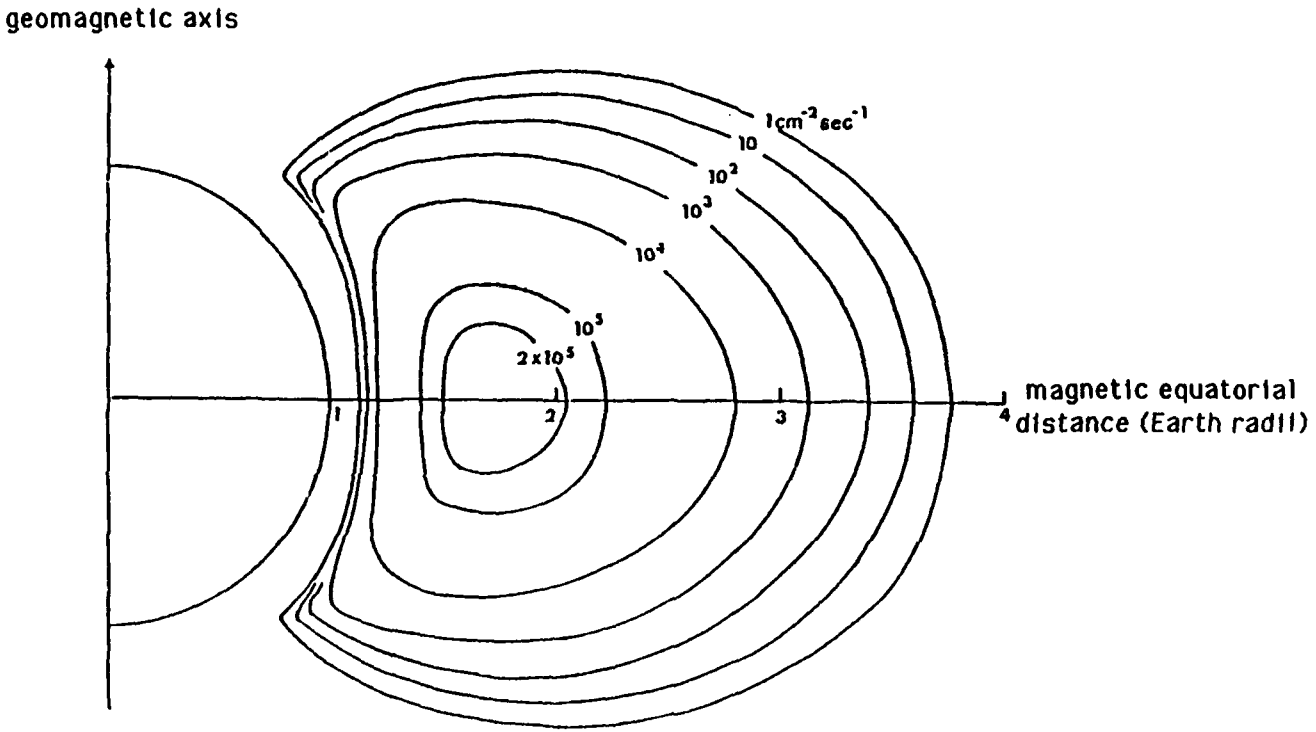

Fig 2 Contours of constant proton flux (>10 MeV) observed in a plane containing the geomagnetic (North-South) axis

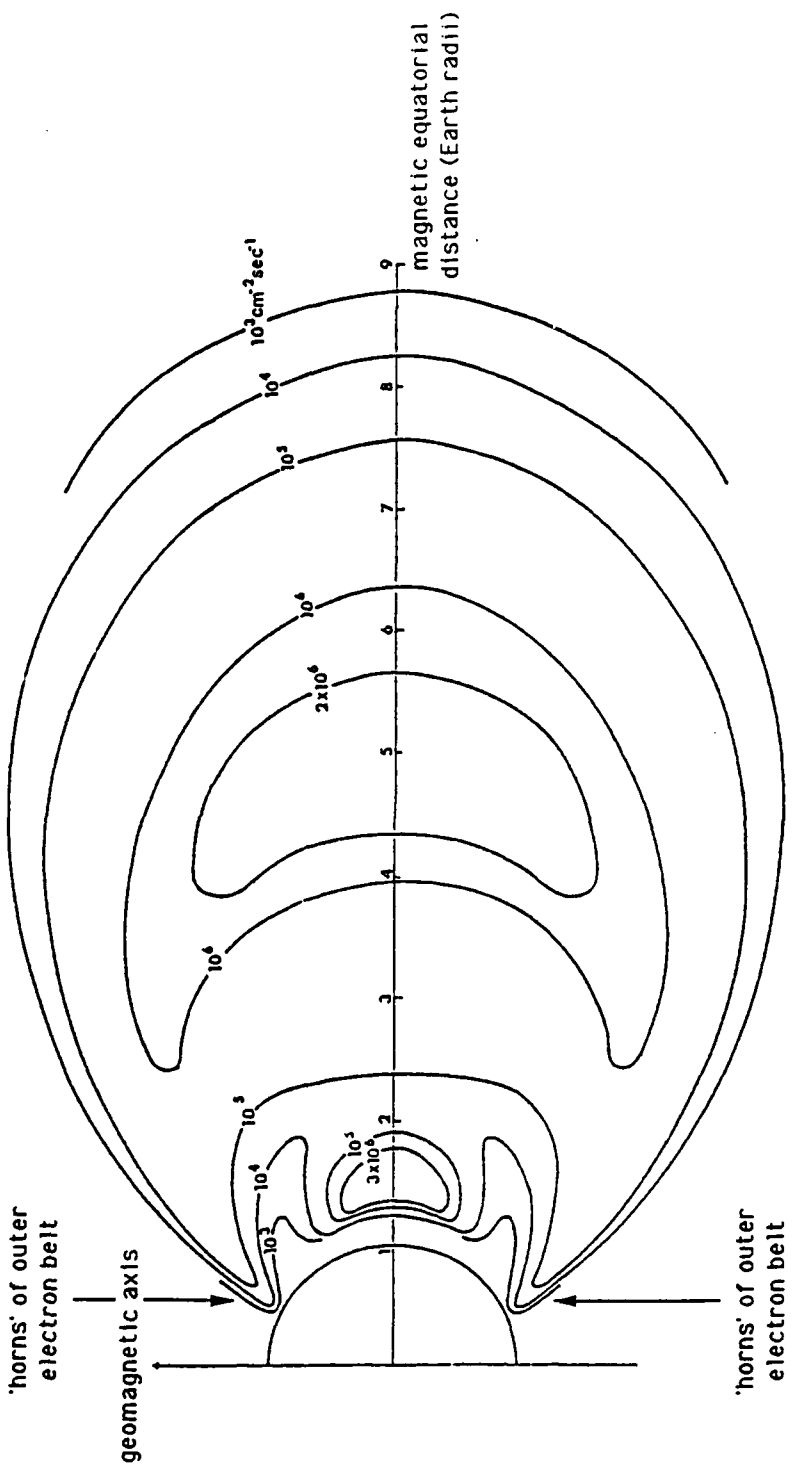

Fig 3 Contours of constant electron flux (>1 MeV) observed in a plane containing the geomagnetic (North-South) axis

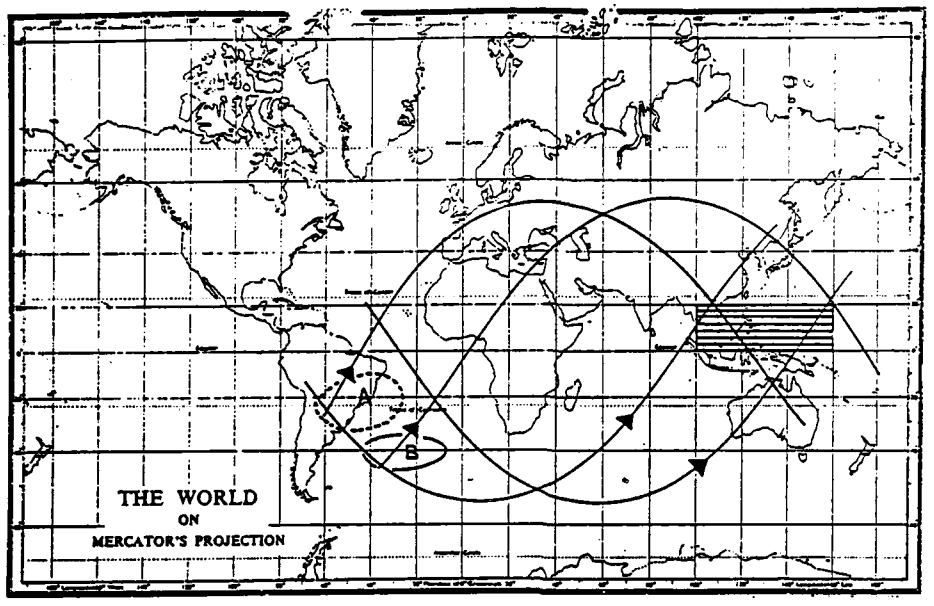

Fig 4 Projection on the Earth's surface of four orbital segments passing through the region of enhanced counting rate (Elliot[6])

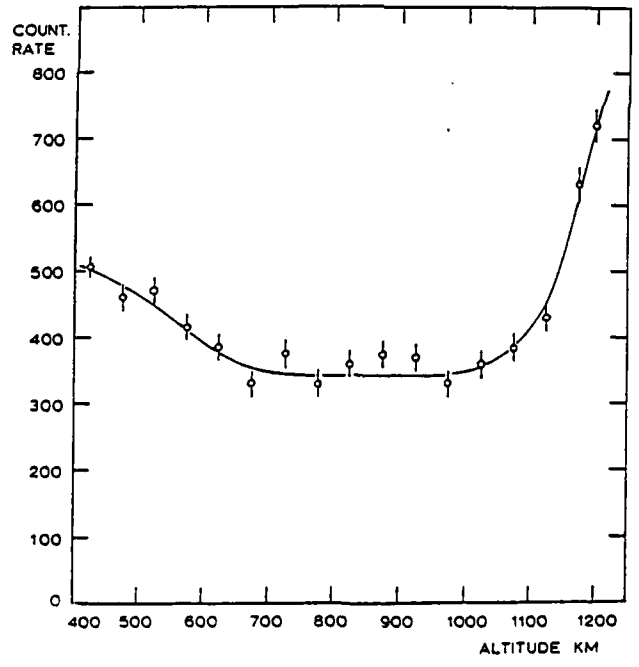

Fig 5 Counting rate of Anton GM-302 as a function of altitude in area bounded by 0°-20° N latitude and 100°-130° longitude (Elliot[6])

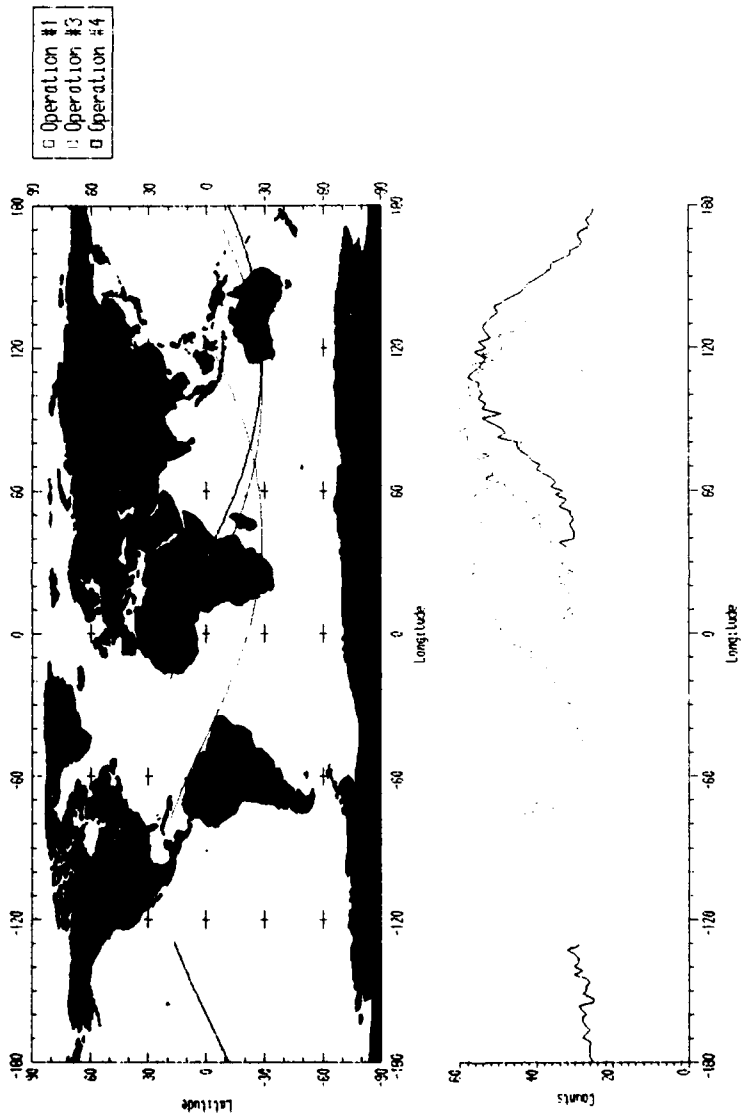

Fig 6 HRM-III data plotted as a function of geographical longitude Shuttle mission STS-41B

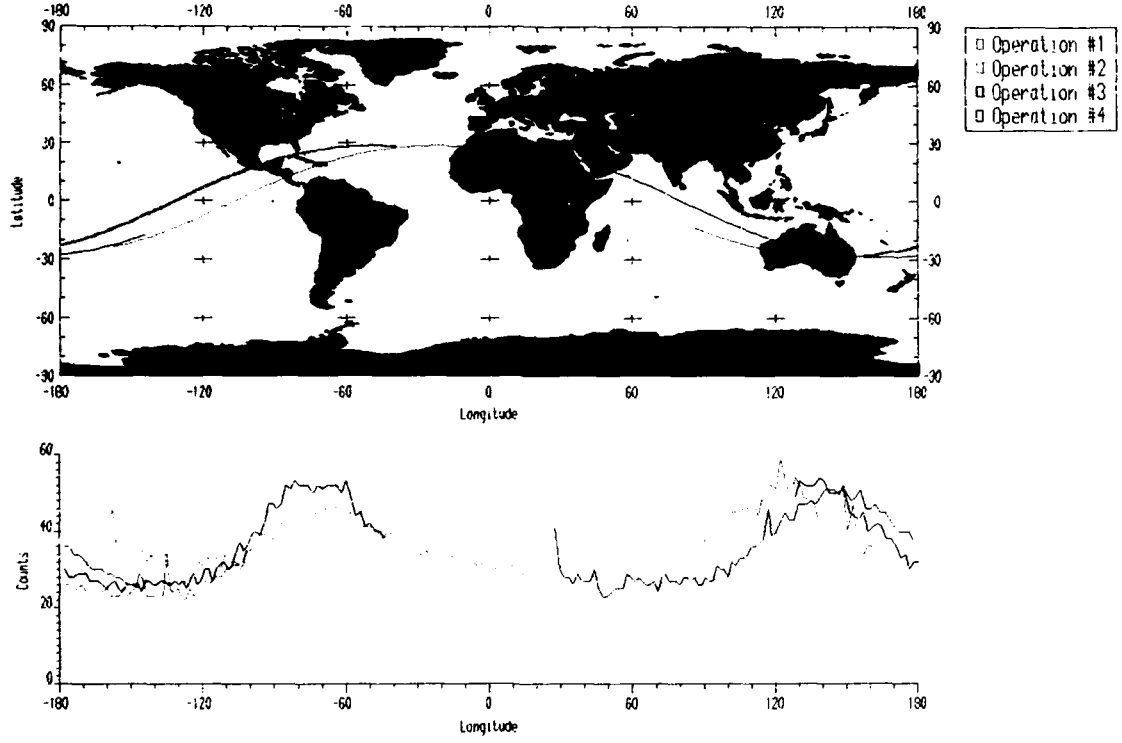

Fig 7 HRM-III data plotted as a function of geographical longitude Shuttle mission STS-41C

Fig 7

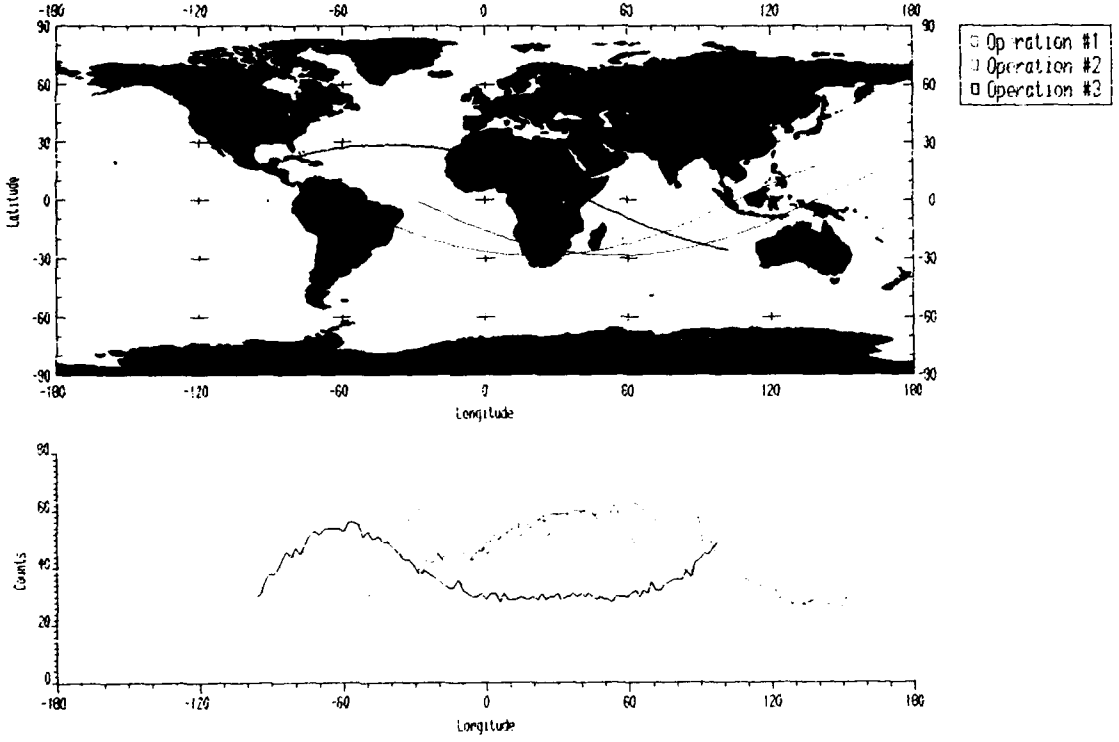

Fig 8 HRM-III data plotted as a function of geographical longitude Shuttle mission STS-41D

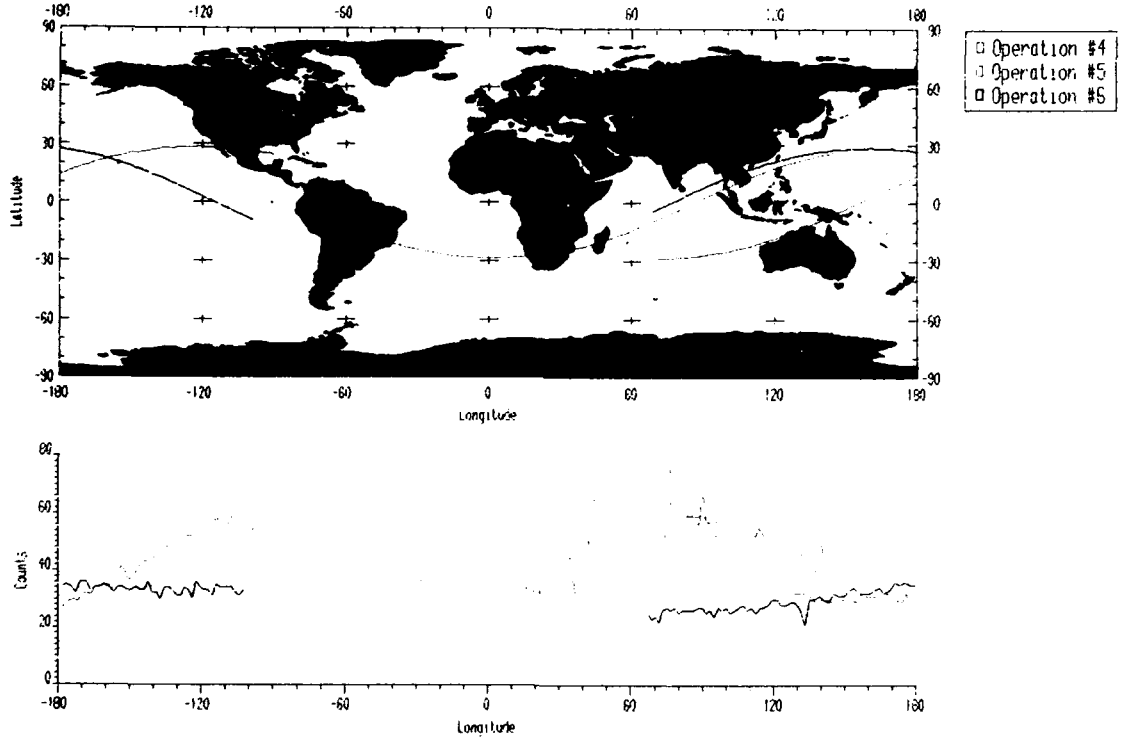

Fig 9 HRM-III data plotted as a function of geographical longitude Shuttle mission STS-41D

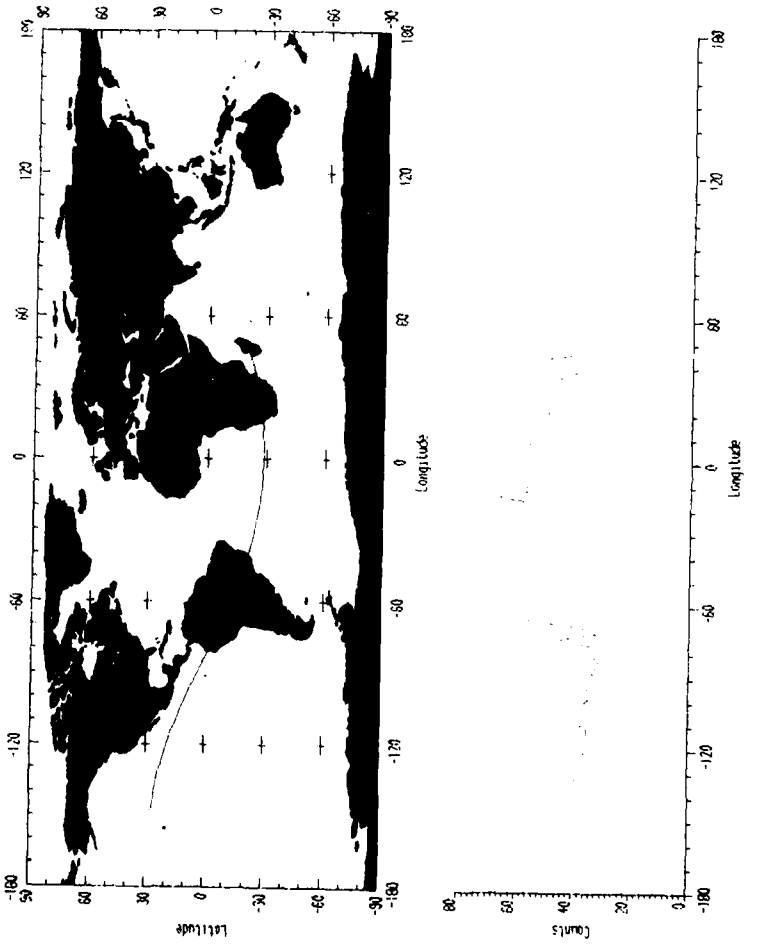

Fig 10 HRM-III data plotted as a function of geographical longitude
Shuttle mission STS-41B
HRM-III Operation #5

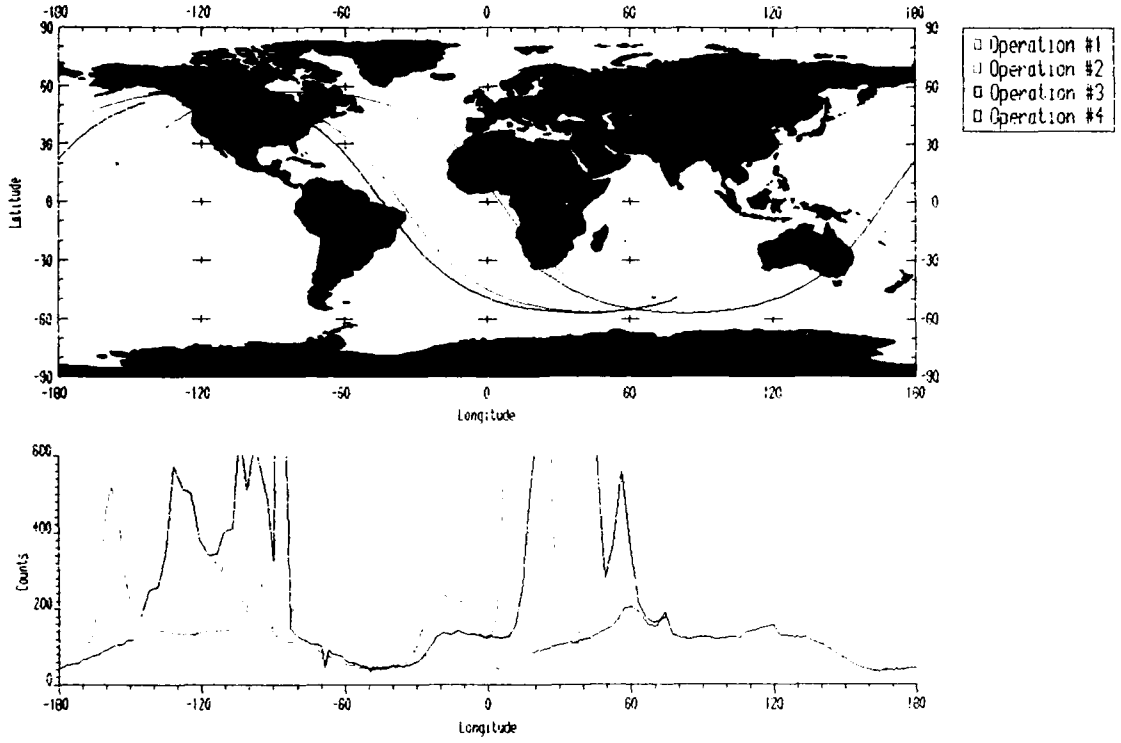

Fig 11 HRM-III data plotted as a function of geographical longitude Shuttle mission STS-41G

Fig 11

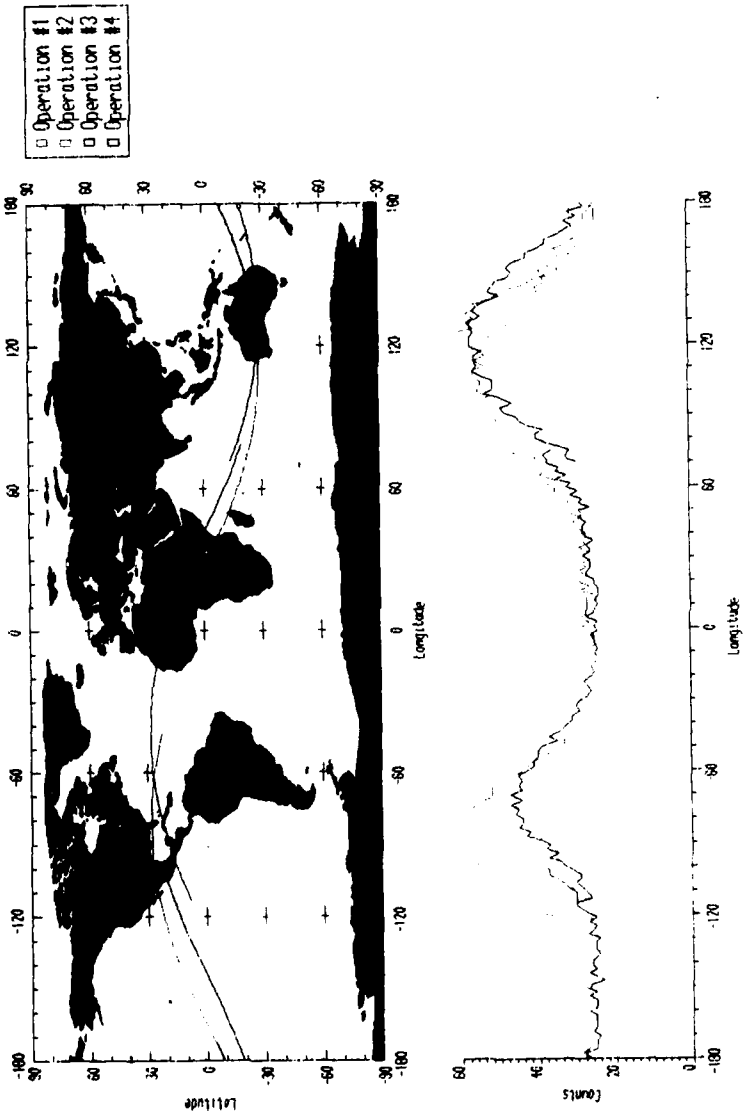

Fig 12 HRM-III data plotted as a function of geographical longitude
Shuttle mission STS-51A

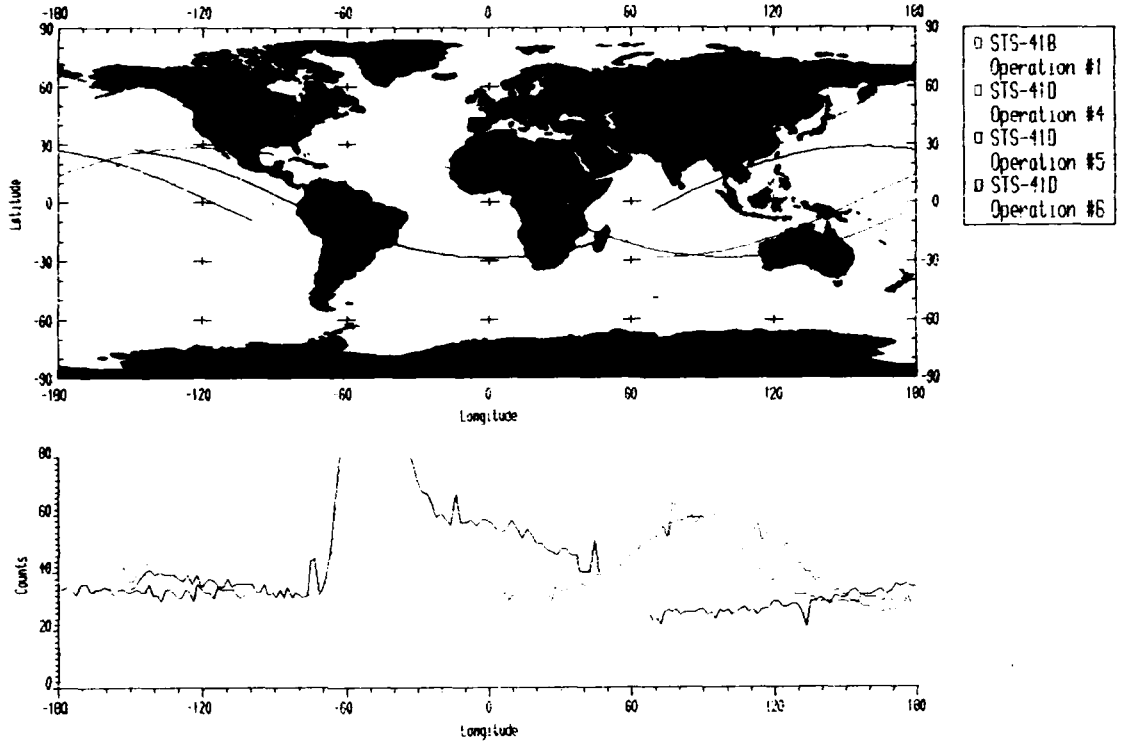

Fig 13 HRM-III data plotted as a function of geographical longitude
Detector operations where SEAA effects were noticed in the previous analysis

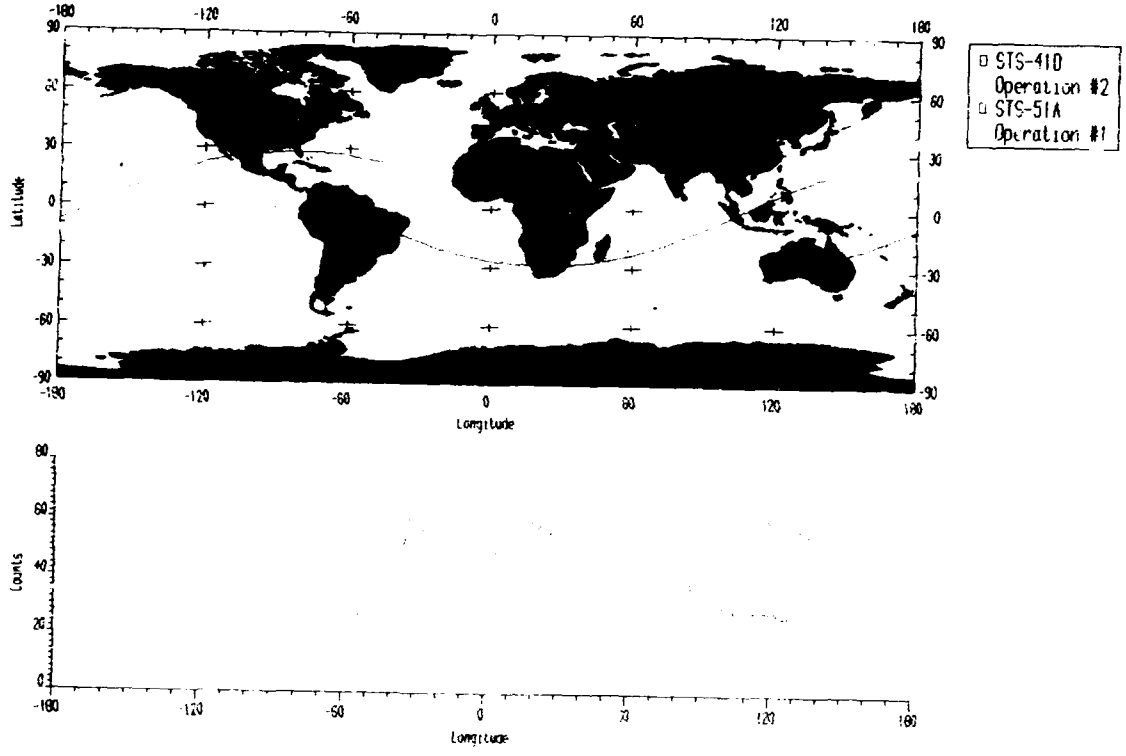

Fig 14 HRM-III data plotted as a function of geographical longitude Detector operations where other discrepancies were noticed in the previous analysis

Fig 14

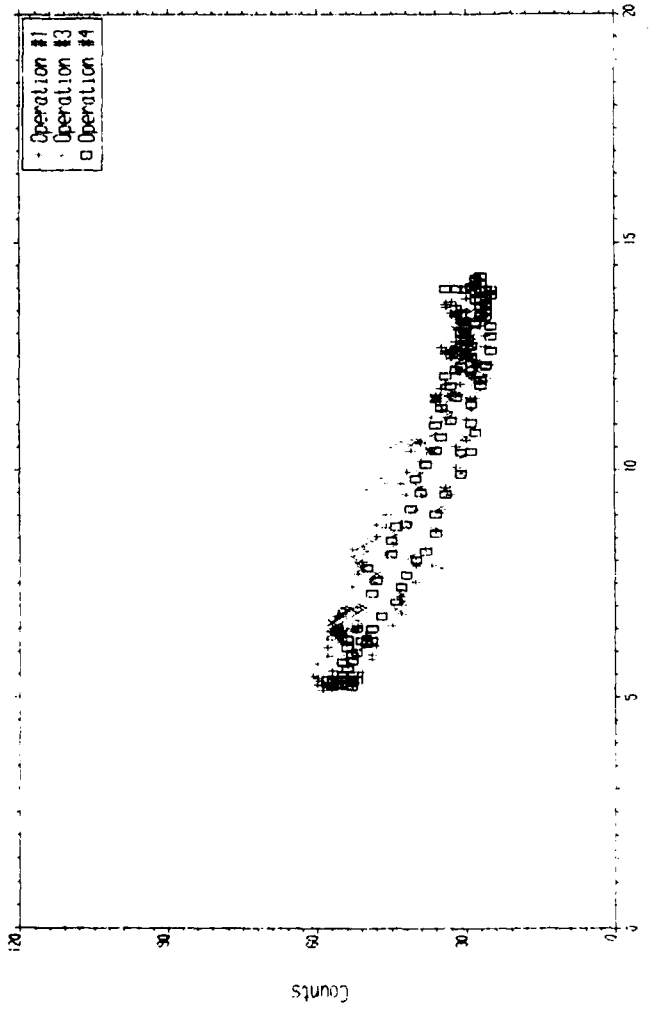

Fig 15 HRM-III data plotted as a function of vertical cut-off rigidity Shuttle mission STS-41B

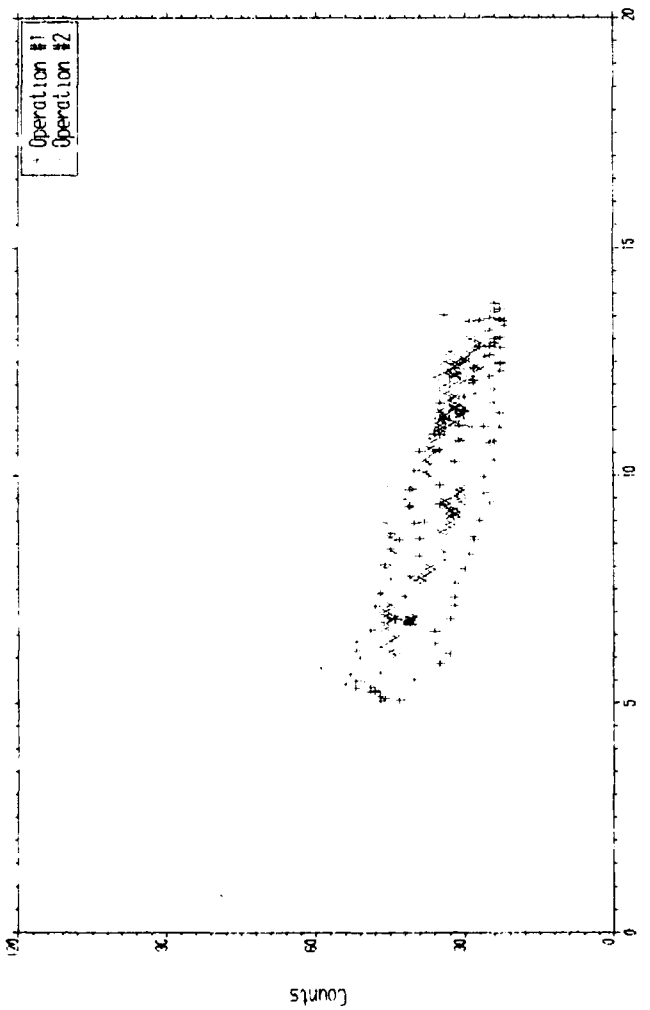

Fig 16 HRM-III data plotted as a function of vertical cut-off rigidity Shuttle mission STS-41C

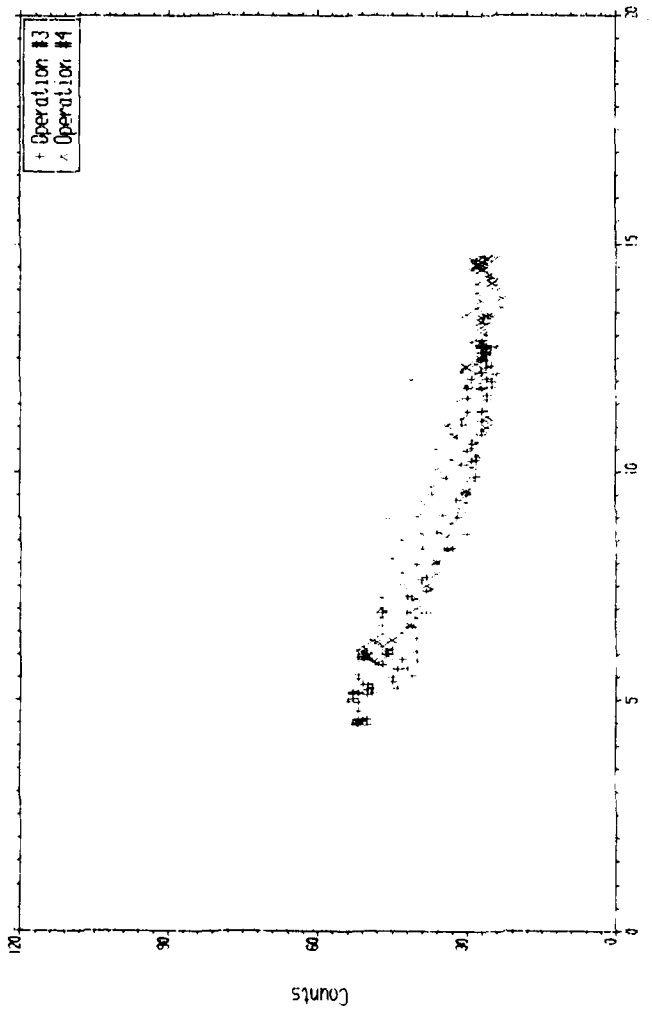

Fig 17 HRM-III data plotted as a function of vertical cut-off rigidity Shuttle mission STS-41C

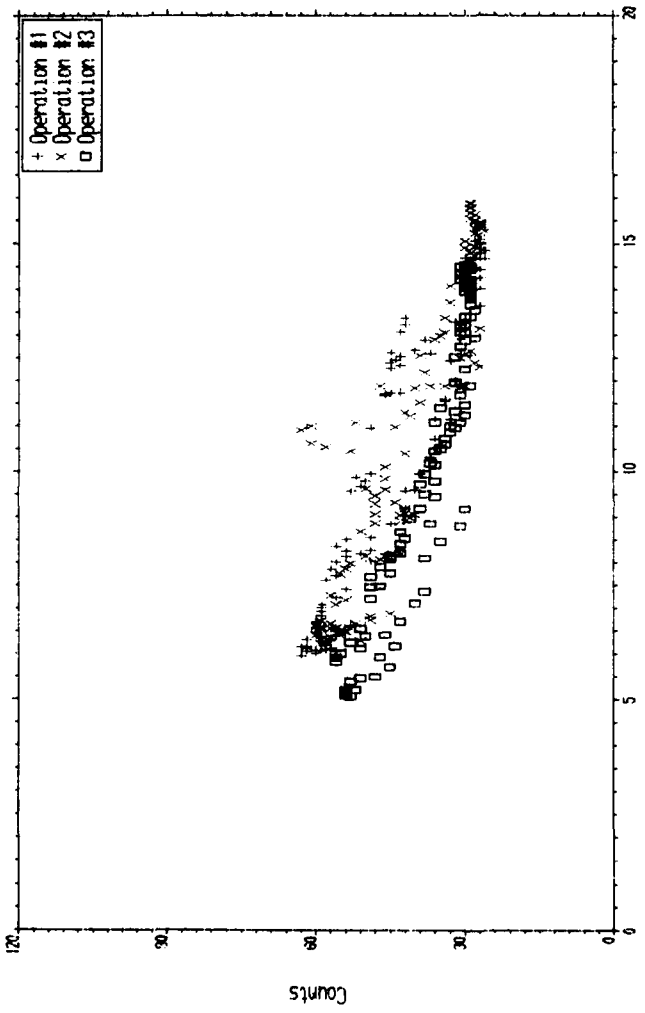

Fig 18 HRM-III data plotted as a function of vertical cut-off rigidity
Shuttle mission STS-41D

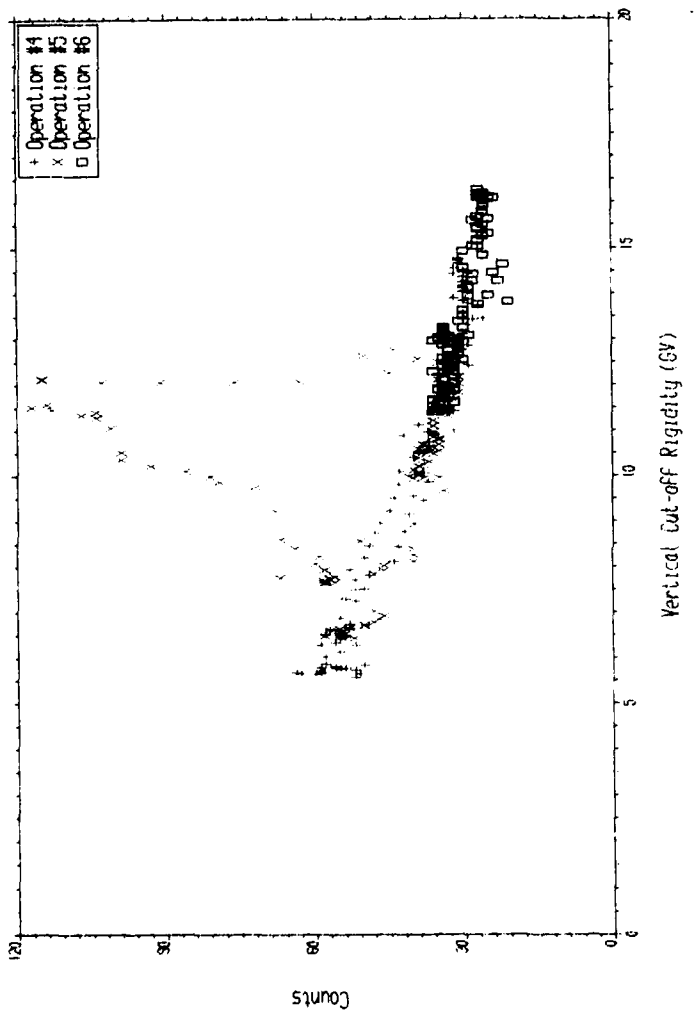

Fig 19 HRM-III data plotted as a function of vertical cut-off rigidity
Shuttle mission STS-41D

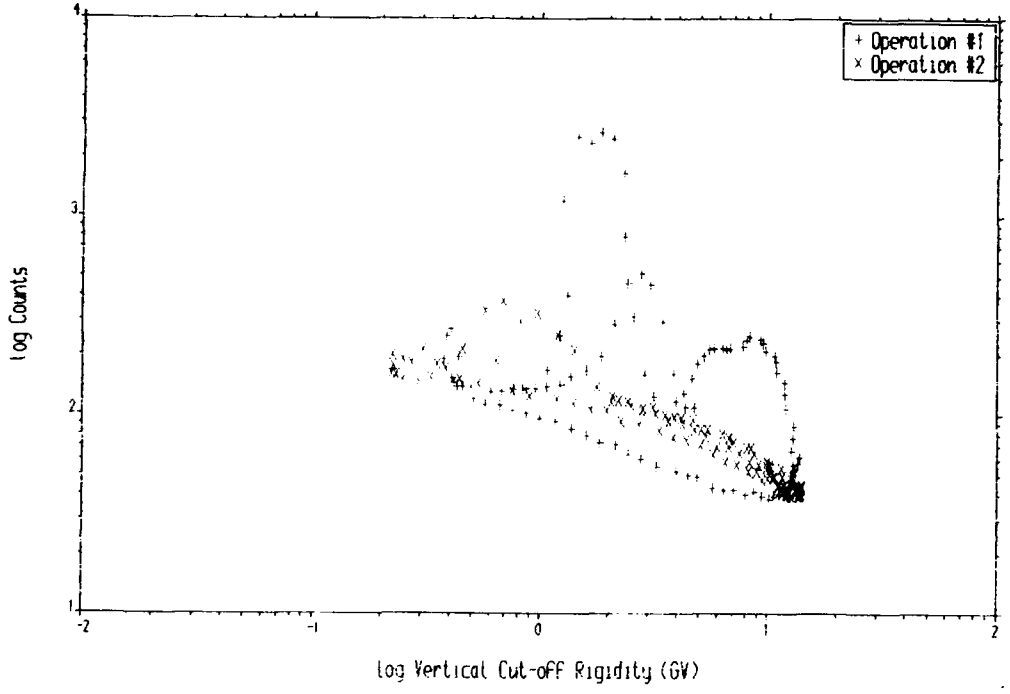

Fig 20 HRM-III data plotted as a function of vertical cut-off rigidity Shuttle mission STS-41G

Fig 20

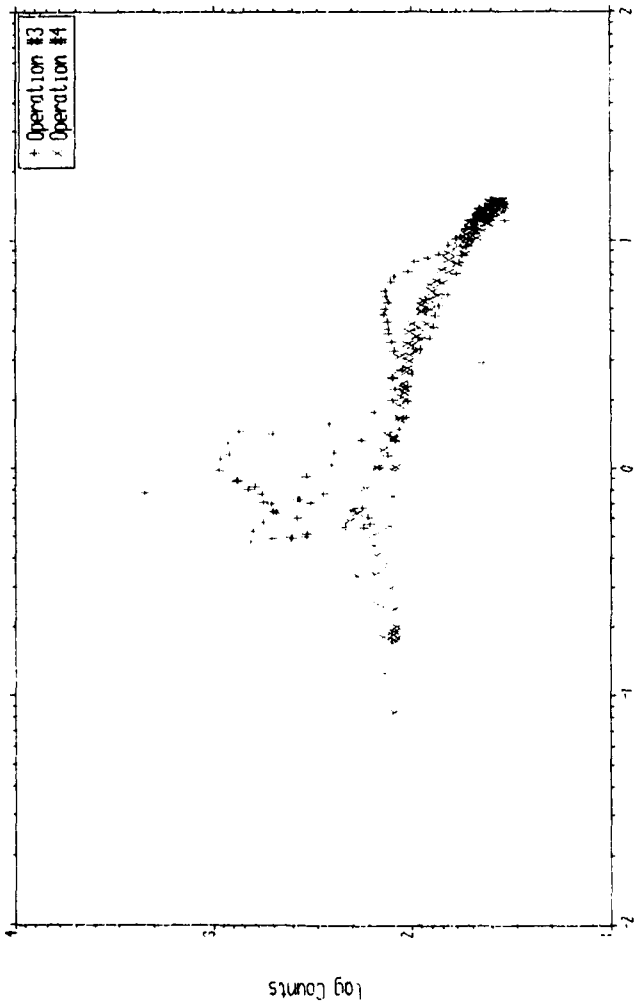

Fig 21 HRM-III data plotted as a function of vertical cut-off rigidity Shuttle mission STS-41G

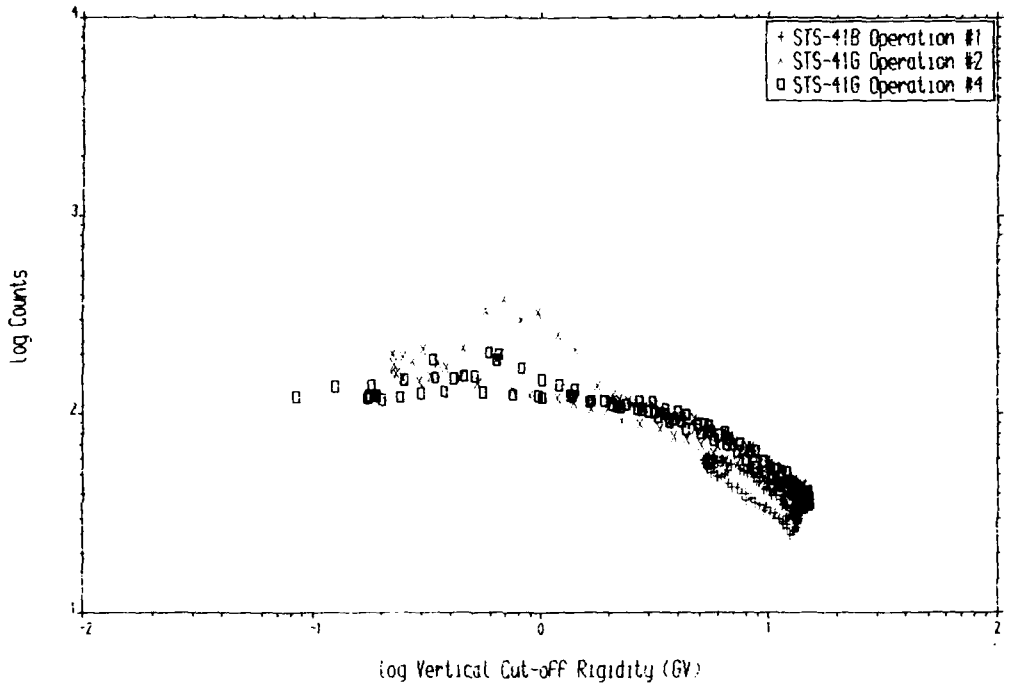

Fig 22 HRM-III data plotted as a function of vertical cut-off rigidity Shuttle mission STS-41B and STS-41G

Fig 22

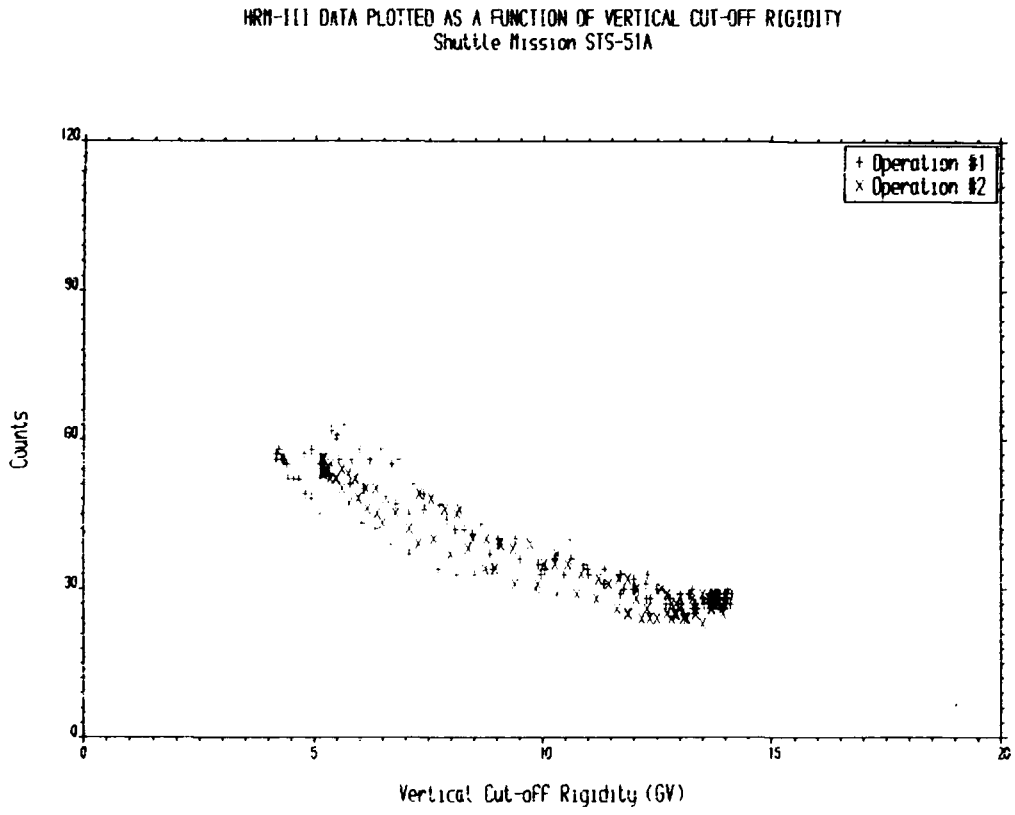

Fig 23 HRM-III data plotted as a function of vertical cut-off rigidity Shuttle mission STS-51A

Fig 23

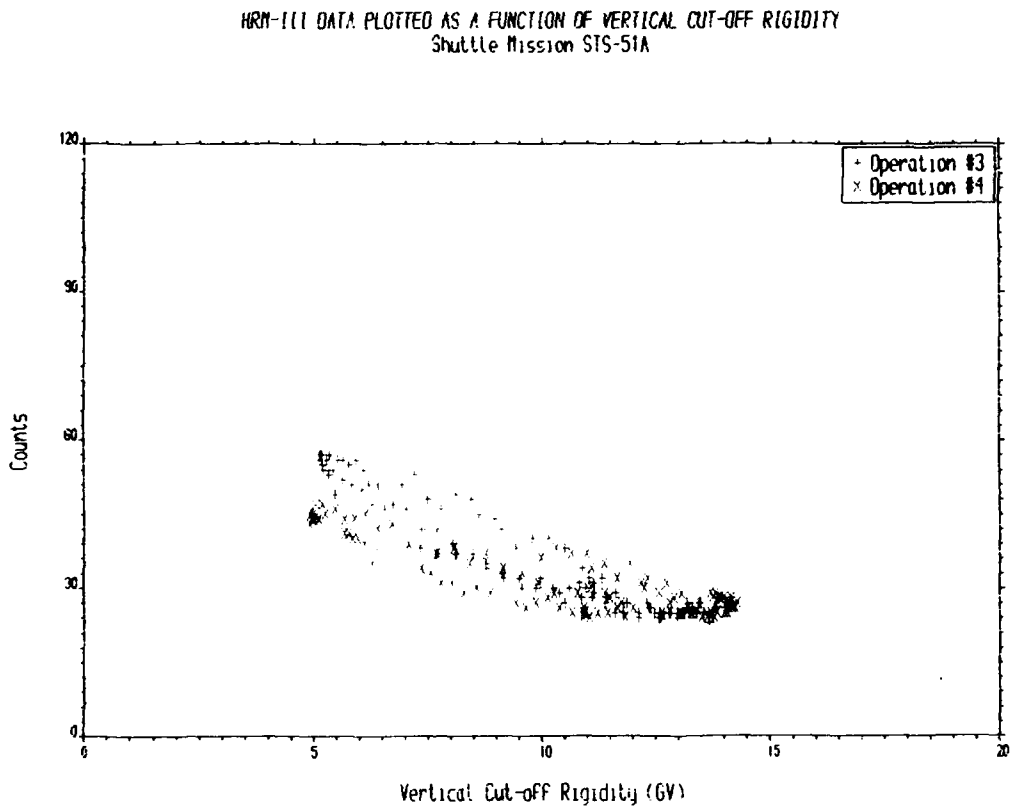

Fig 24 HRM-III data plotted as a function of vertical cut-off rigidity Shuttle mission STS-51A

Fig 24

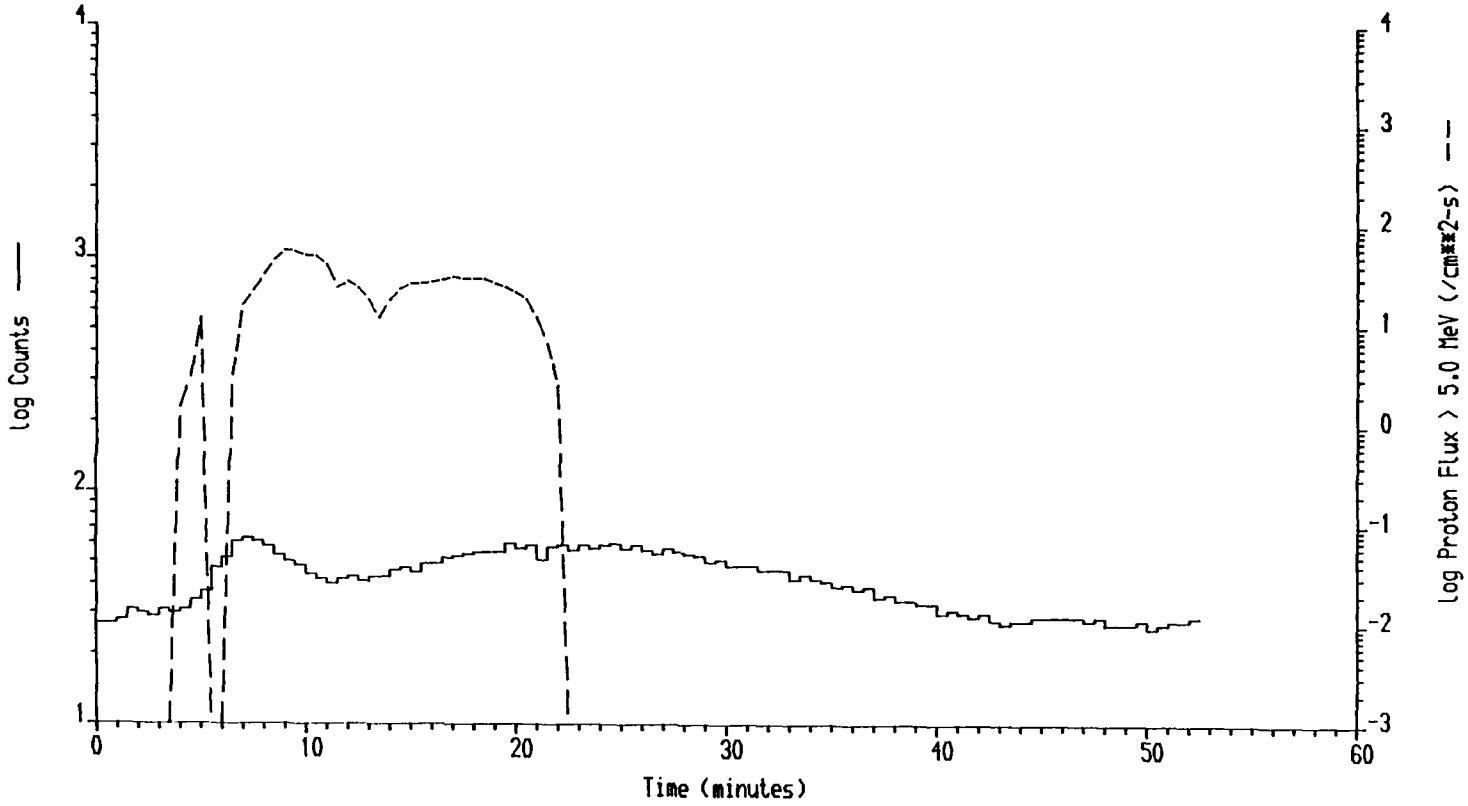

Fig 25 Comparison of HRM-III data and predicted trapped proton flux
Shuttle mission STS-41D
HRM-III operation #2

Fig 25

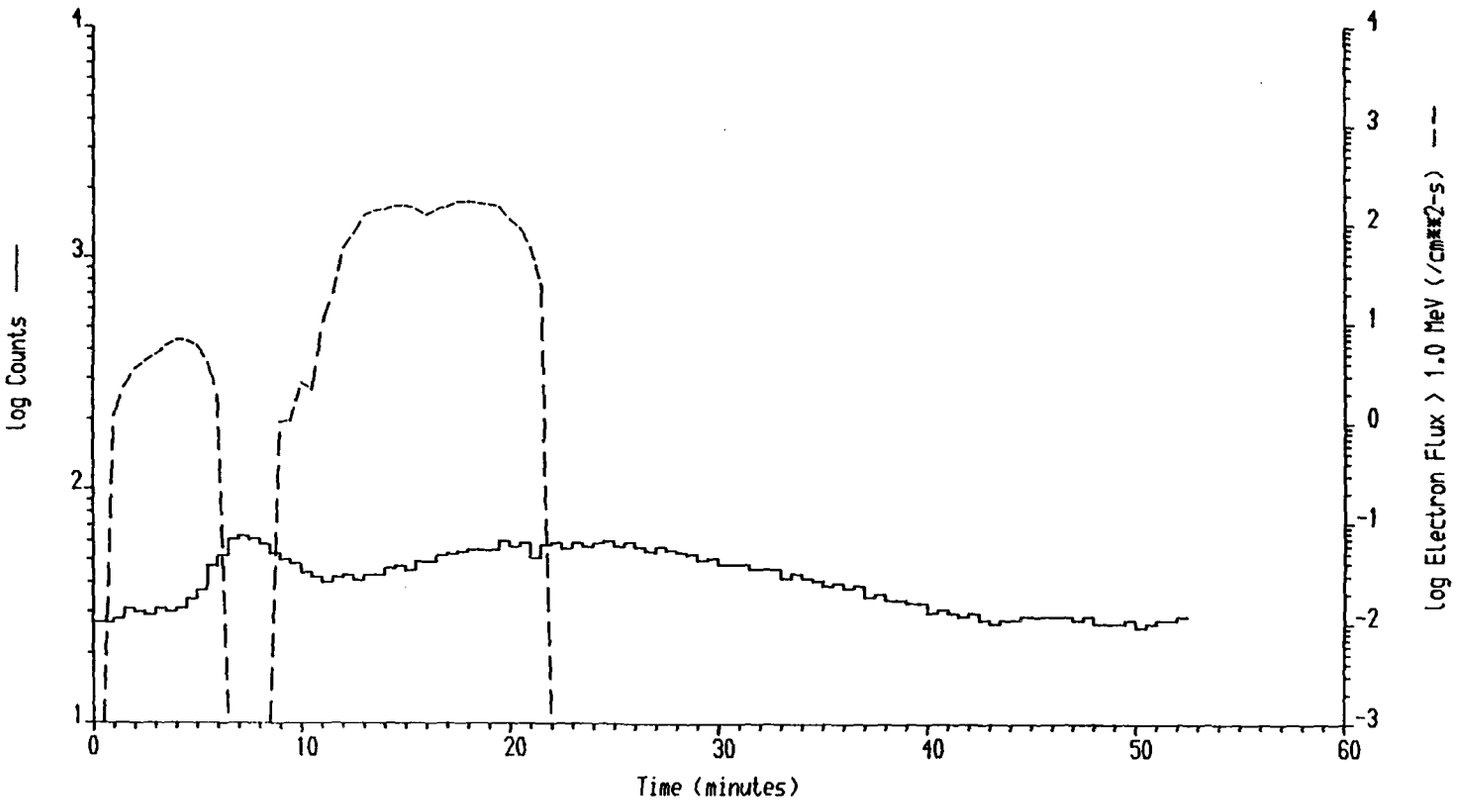

Fig 26 Comparison of HRM-III data and predicted trapped electron flux
Shuttle mission STS-41D
HRM-III operation #2

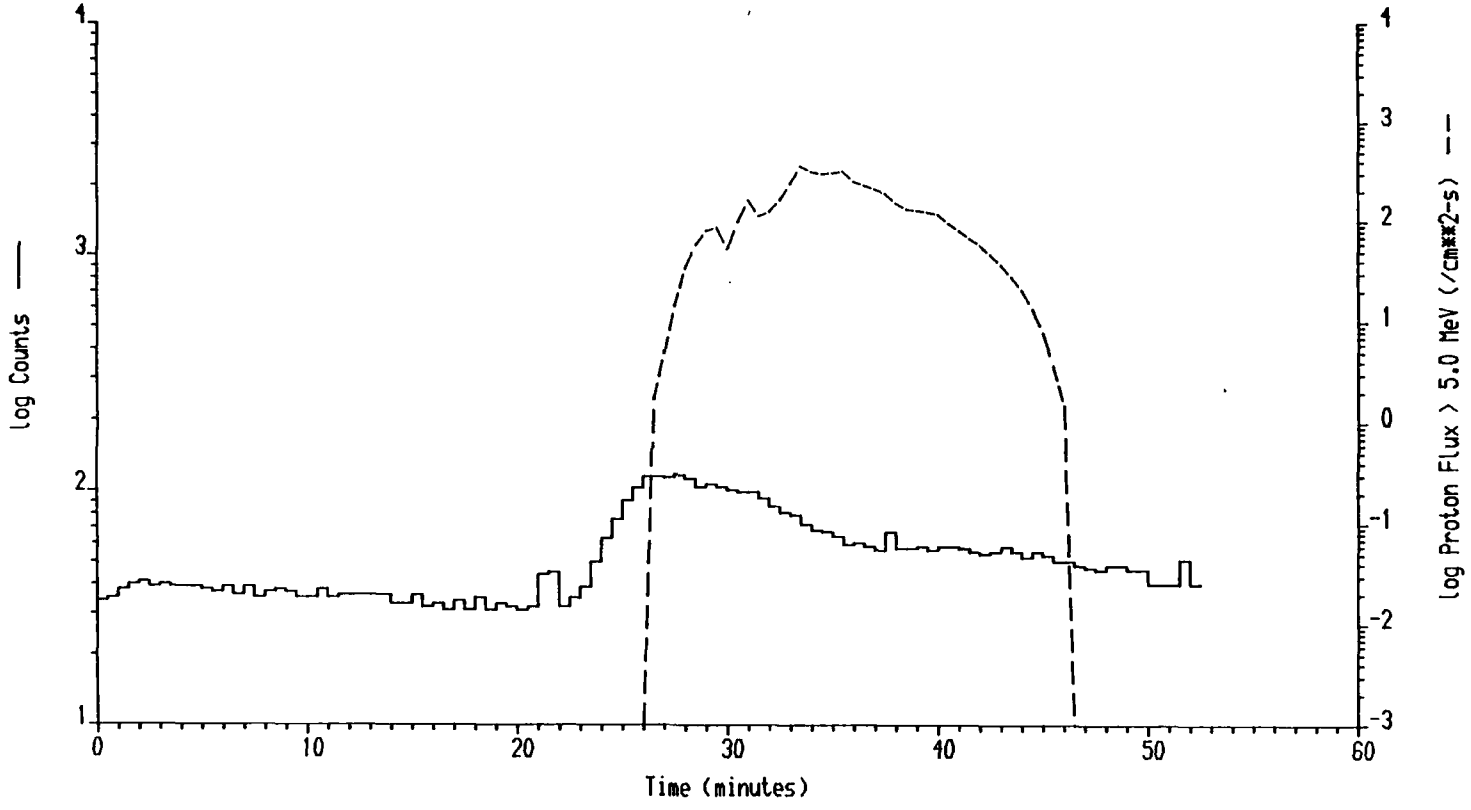

Fig 27 Comparison of HRM-III data and predicted trapped proton flux
Shuttle mission STS-41D
HRM-III operation #5

Fig 27

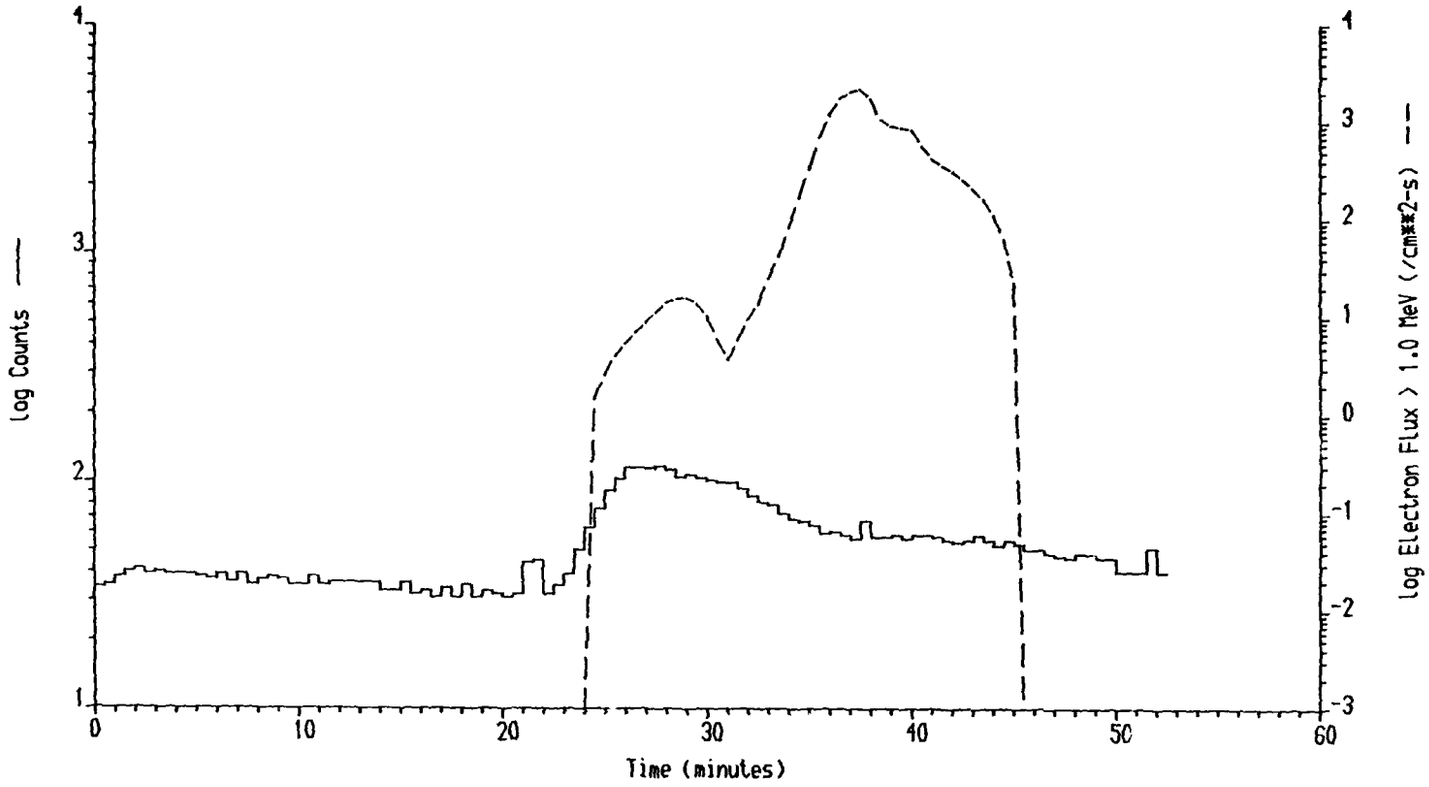

Fig 28 Comparison of HRM-III data and predicted trapped electron flux
Shuttle mission STS-41D
HRM-III operation #5

TR 89048

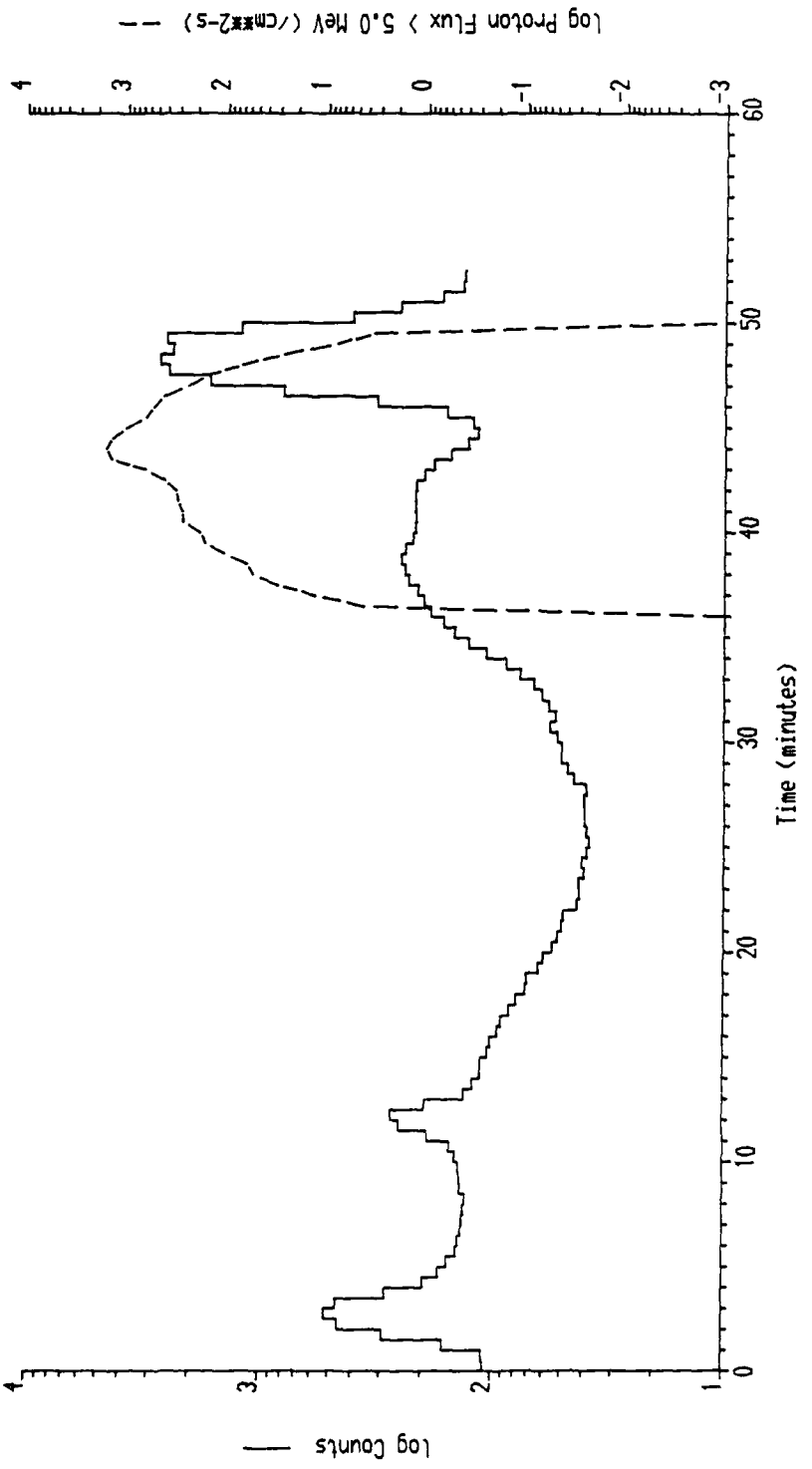

Fig 29 Comparison of HRM-III data and predicted trapped proton flux
Shuttle mission STS-41G
HRM-III operation #1

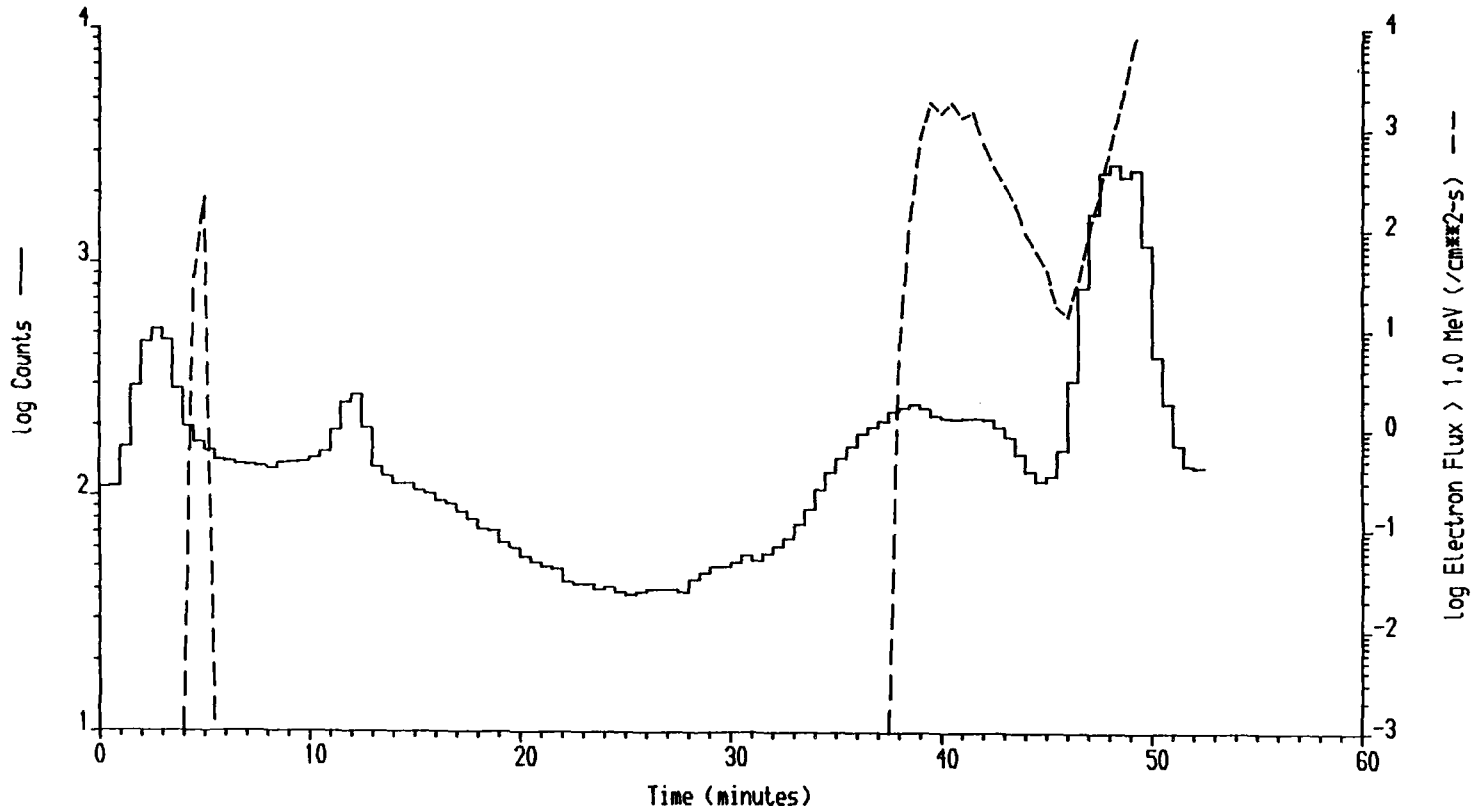

Fig 30 Comparison of HRM-III data and predicted trapped electron flux
Shuttle mission STS-41G
HRM-III operation #1

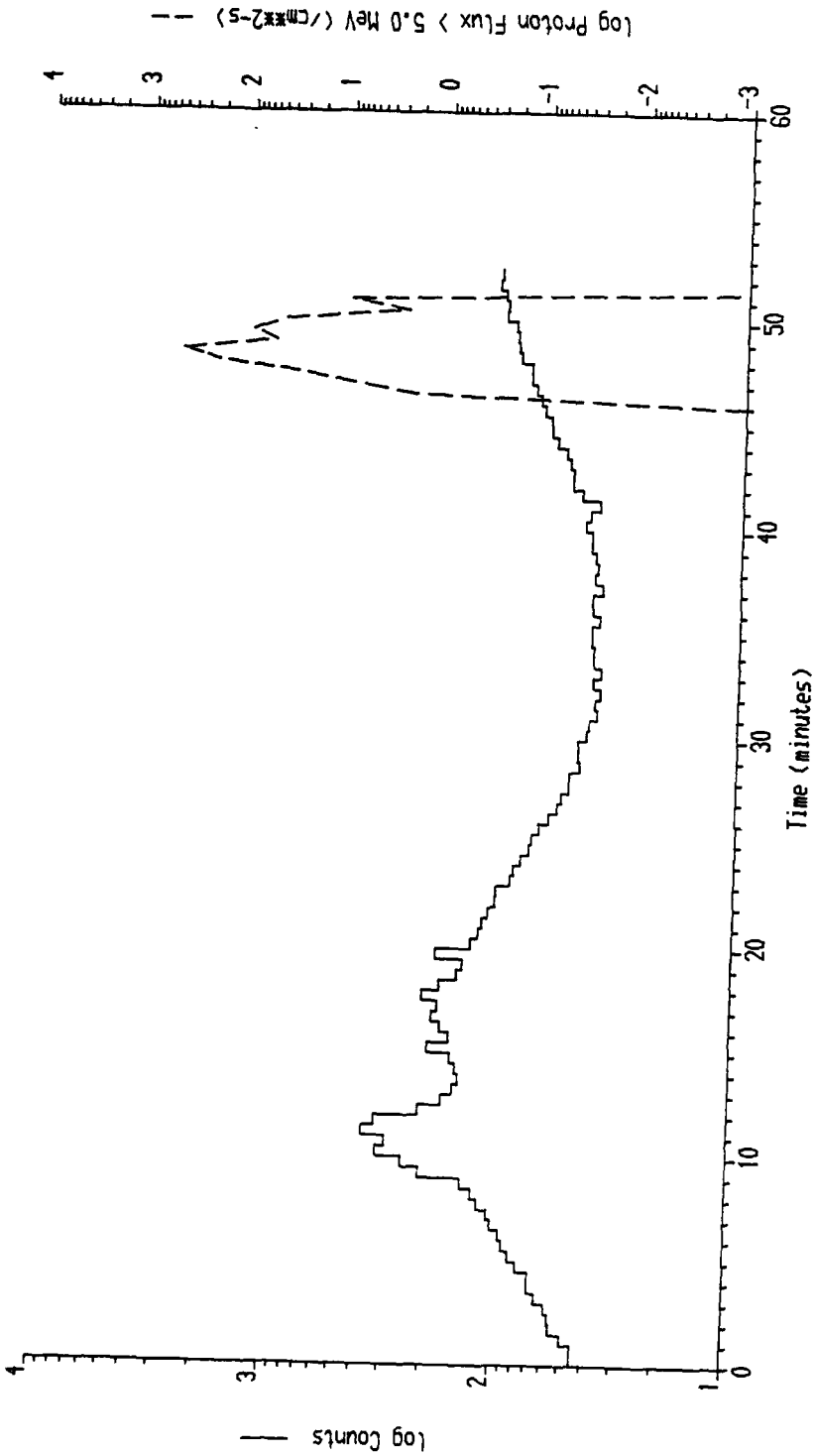

Fig 31 *Comparison of HRM-III data and predicted trapped proton flux*
Shuttle mission STS-41G
HRM-III operation #2

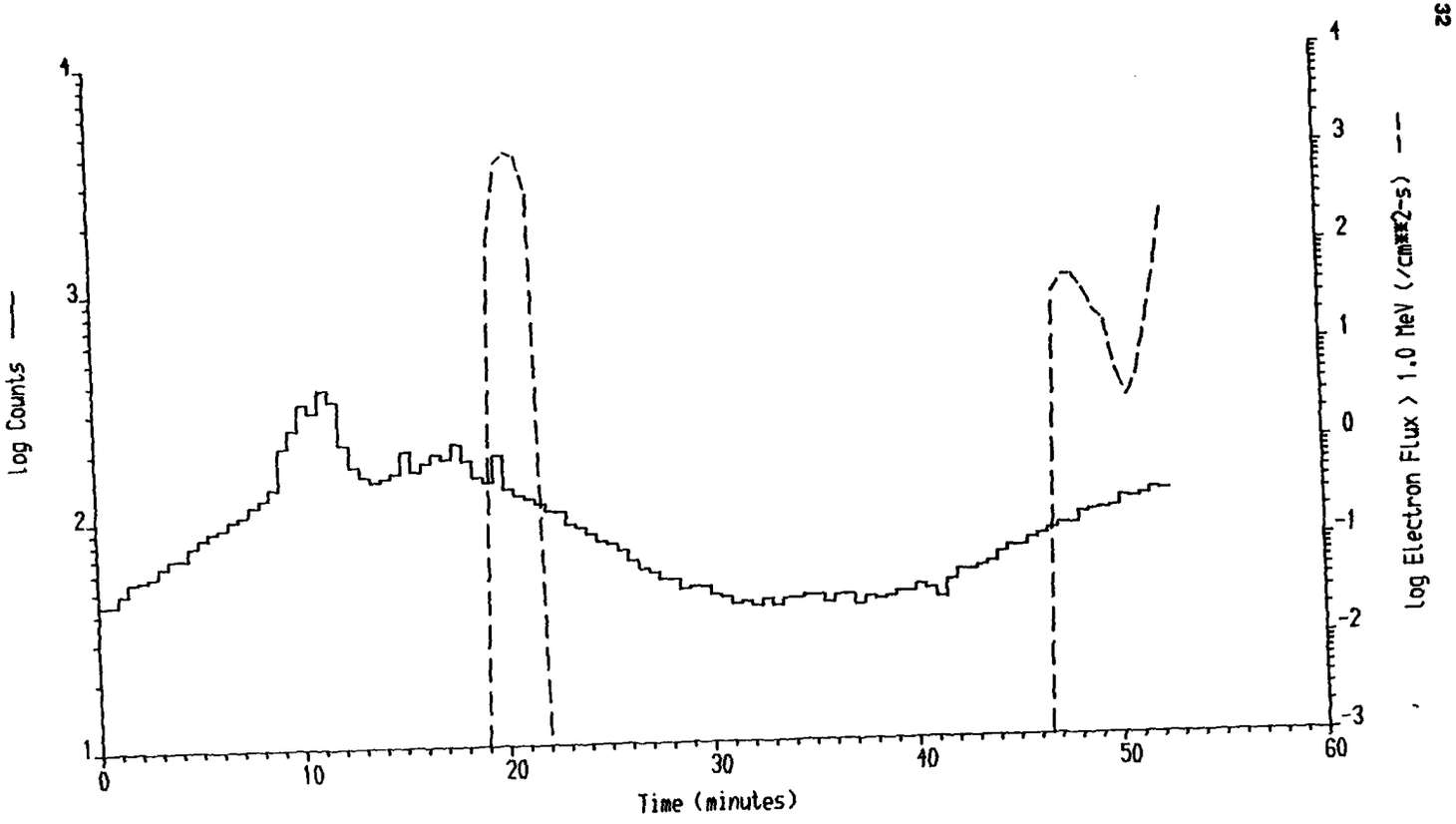

Fig 32 Comparison of HRM-III data and predicted trapped electron flux
Shuttle mission STS-41G
HRM-III operation #2

TR 89048

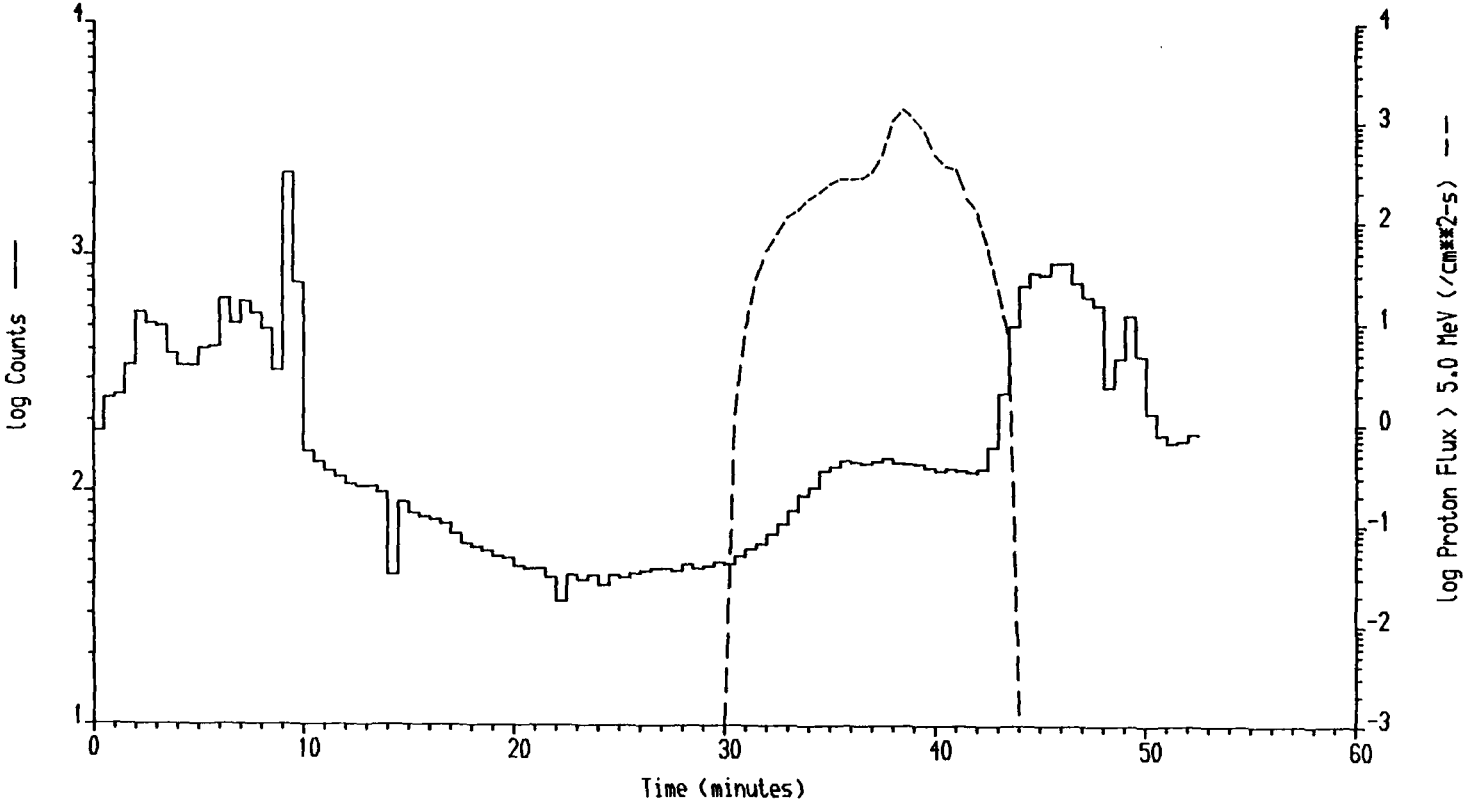

Fig 33 Comparison of HRM-III data and predicted trapped proton flux
Shuttle mission STS-41G
HRM-III operation #3

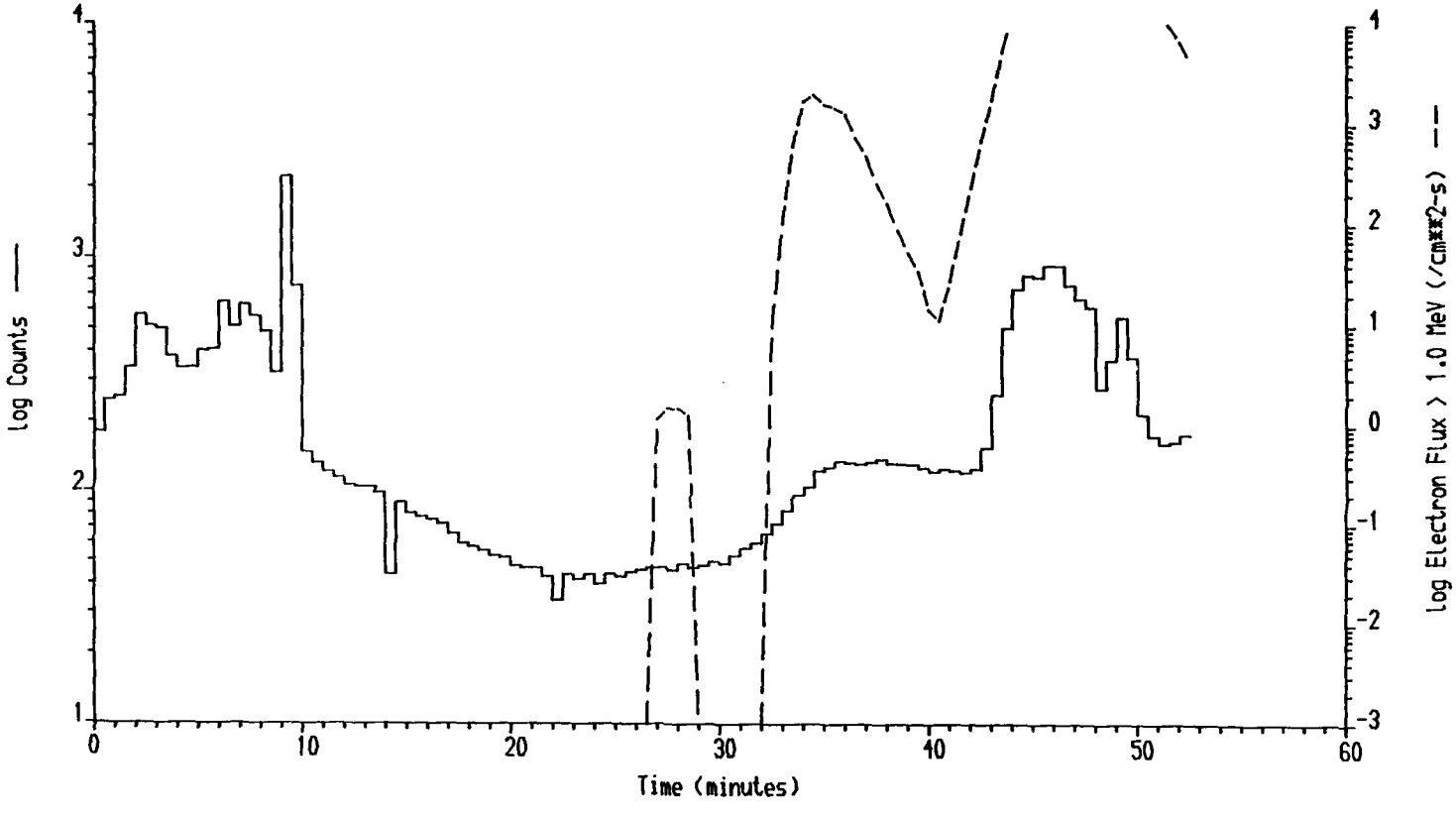

Fig 34 Comparison of HRM-III data and predicted trapped electron flux
Shuttle mission STS-41G
HRM-III operation #3

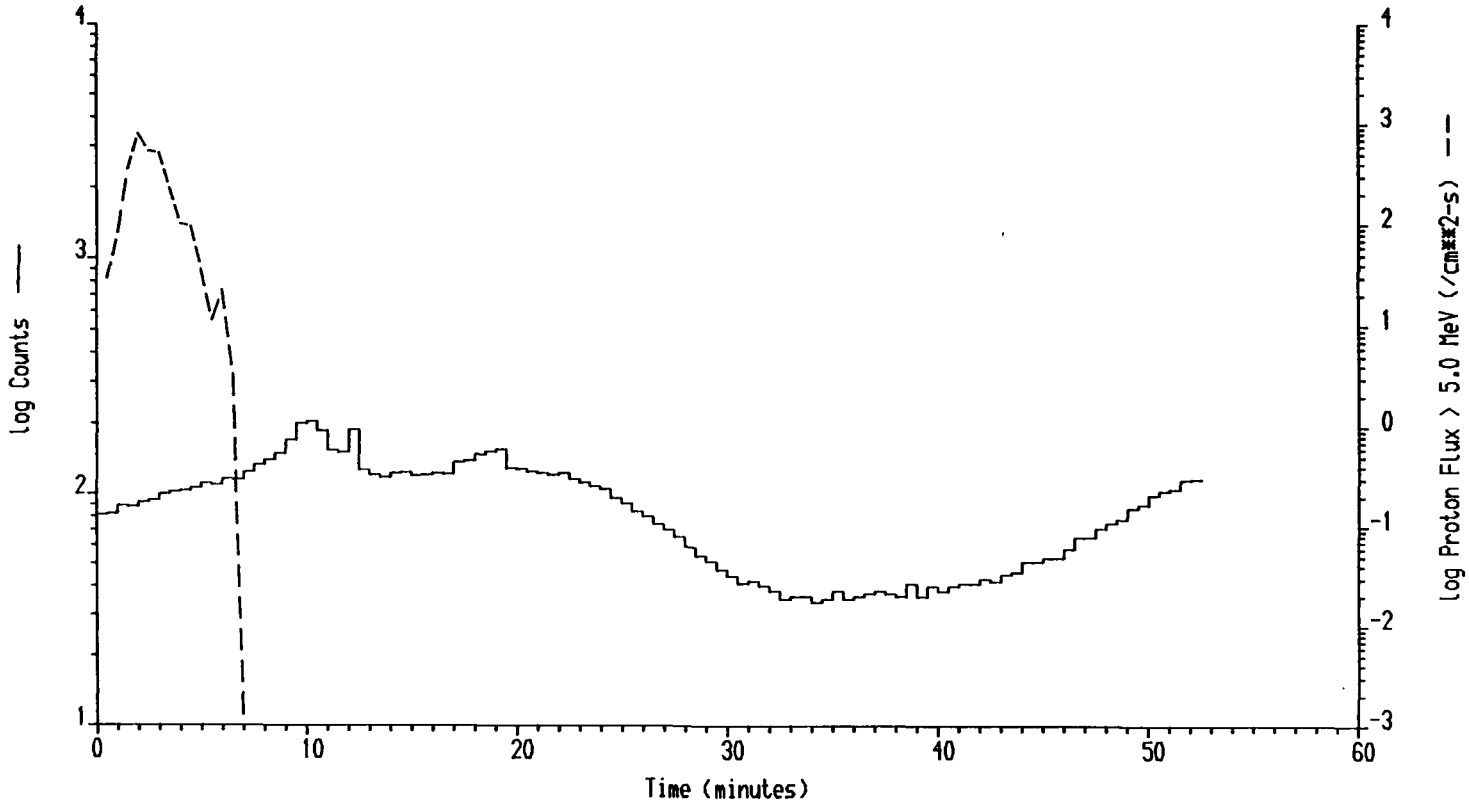

Fig 35 Comparison of HRM-III data and predicted trapped proton flux
Shuttle mission STS-41G
HRM-III operation #4

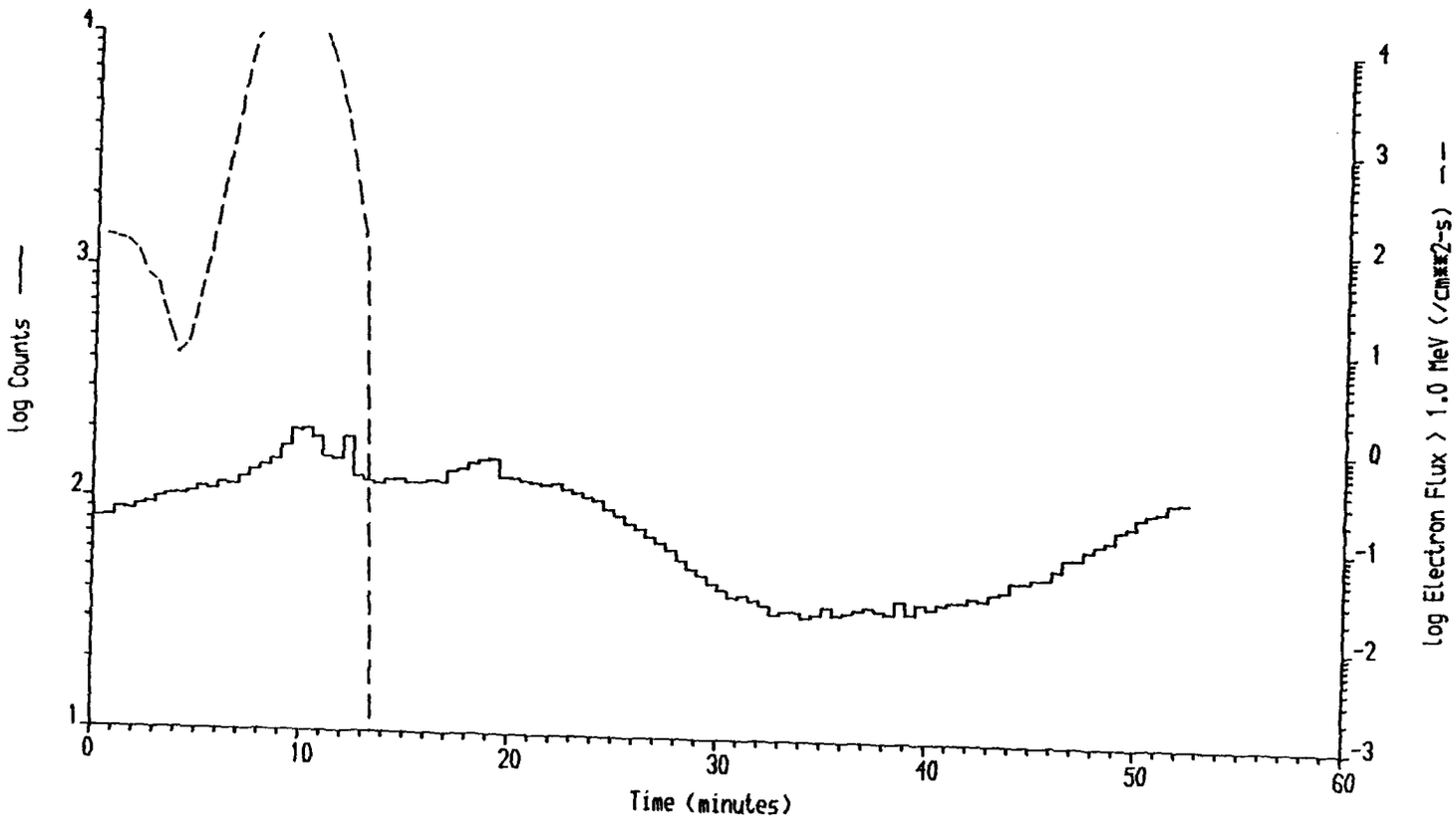

Fig 36

Fig 36 Comparison of HRM-III data and predicted trapped electron flux
Shuttle mission STS-41G
HRM-III operation #4

TR 89048

REPORT DOCUMENTATION PAGE

Overall security classification of this page

Instructions for completion appear overleaf. UNLIMITED

As far as possible this page should contain only unclassified information. If it is necessary to enter classified information, the box above must be marked to indicate the classification, e.g. Restricted, Confidential or Secret.

1. DRIC Reference (to be added by DRIC)	2. Originator's Reference	3. Agency Reference	4. Report Security Classification/Marking
	RAE TR 89048		UNLIMITED

5. DRIC Code for Originator	6. Originator (Corporate Author) Name and Location
7673000W	Royal Aerospace Establishment, Farnborough, Hants, UK
5a. Sponsoring Agency's Code	6a. Sponsoring Agency (Contract Authority) Name and Location

7 Title Re-analysis of data on the space radiation environment above South-East Asia

7a. (For Translations) Title in Foreign Language

7b. (For Conference Papers) Title, Place and Date of Conference

8. Author 1. Surname, Initials	9a. Author 2	9b. Authors 3, 4	10. Date	Pages	Refs.
Truscott P.R.			Sept 1989	60	16

11. Contract Number	12. Period	13. Project	14. Other Reference Nos.
			Space 677

15. Distribution statement

(a) Controlled by –

(b) Special limitations (if any) –

If it is intended that a copy of this document shall be released overseas refer to RAE Leaflet No.3 to Supplement 6 of MOD Manual 4.

16. Descriptors (Keywords) (Descriptors marked * are selected from TEST)

South-East Asian Anomaly. Radiation belts, Space Shuttle, Cosmic rays, Radiation monitoring, Trapped radiation. HRM-III.

17. Abstract

A new analysis has been performed on the HRM-III gamma ray detector data collected from Shuttle missions STS-41B, 41C, 41D, 41G and 51A. The new analysis shows no evidence for the existence of enhanced levels of radiation in low-Earth orbit over South-East Asia (ie in the area bounded by longitudes 100°E to 190°E and latitudes 10°S to 15°N) as previously suggested. Variations in the detector count rates with geographical location are shown to be consistent with the variation of the cosmic ray flux with geomagnetic latitude, and also show expected increases due to the South Atlantic Anomaly (SAA) and outer belt electrons. However, at times poor quantitative agreement is found between the expected positions of the SAA or outer electron belt, and the Shuttle's geographical location on the occasions when high count rates were observed. It is believed that this lack of correlation is a result of the sensitivity of the trapped particle environment to geographical position and magnetospheric activity.

F5510/1

RAE Form A143 (revised October 1980)